BSGF - Earth Sciences Bulletin 2026, 197, 5
© M. Mombo Mouketo *et al.*, Published by EDP Sciences 2026
https://doi.org/10.1051/bsgf/2025028

BSGF Earth Sciences Bulletin
Available online at:
www.bsgf.fr

De la géologie structurale à la géodynamique : un numéro thématique dédié à la contribution de l'école rennaise de tectonique - Hommage à J-P Brun, P. Choukroune et P.R. Cobbold
Frédéric Gueydan and Dominique Chardon (Guest editors)

Open Access

Structural organization of the Lorraine coal basin and formation of the Alsting thrust fold

Metzger Mombo Mouketo[1,*], Yves Géraud[1], Marc Diraison[1], Salim Allouti[1], Alain Izart[1], Khalid Essa[1,2], Claire Bossennec[3] and Fady Nassif[4]

[1] Université de Lorraine, CNRS, Georessources, F-54000 Nancy, France
[2] Geophysics Department, Faculty of Science, Cairo University, Giza, P.O. 12613, Egypt
[3] Université de Lille, Section 36, Terre solide, Géodynamique des enveloppes supérieures Lille, France
[4] La Française de l'Energie (FDE), Pontpierre, France

Received: 6 June 2025 / Accepted: 23 October 2025 / Publishing online: 23 February 2026

Abstract – The Lorraine Coal Basin (LCB), filled with continental clastic formations of the Upper Carboniferous-Permian age, developed along the Metz-Hunsrück-Fault-Zone (MHFZ). Despite the structural studies, the structure of the basement which control the total sedimentary thickness variations, and the Alsting fold structure and formation remains poorly constrained. In this study, the analysis of gravity data has allowed to map the MHFZ and more regionally the top basement structures beneath the basin. The analysis of 2D seismic lines and well data analysis has allowed to constrain the structure and formation of the Alsting fold.
The top basement map highlights the presence of highs (−1, 5 km) and deeps (−6, 5 km) trending NE-SW, NNE-SSW to N-S and NW-SE. This structuration explains the global sedimentary thickness variation of the sedimentary series in place. The first vertical derivative of the Bouger anomaly suggests that the MHFZ is continuous throughout the LCB and the SNCB. Furthermore, seismic interpretations show that the Alsting fold is a thrust fold whose formation and post-compression erosion occurred during the Stephanian. After this deformation phase, subsidence and deposition restarted during the late Stephanian. This study highlights a different Stephanian geological history of the BHL compared with other basins of the same age due to its structural position.

Keywords: Lorraine Coal Basin / basement and basin structure / Stephanian compression / Metz-Hunsrück-Fault-Zone / thickness variations / Alsting thrust-fold formation

Résumé – Organisation structurale du bassin houiller de Lorraine et formation du pli sur chevauchement d'Alsting. Le Bassin Houiller Lorrain (BHL), rempli de formations détritiques continentales d'âge Carbonifère supérieur-Permien, s'est développé le long de la Zone de failles de Metz-Hunsrück. Malgré de nombreuses études structurales, la structure de son socle qui contrôle les variations des épaisseurs des séries sédimentaires et la formation du pli d'Alsting ont très peu été investiguées. Dans cette étude, l'analyse des données gravimétriques a permis de cartographier la zone de faille de Metz-Hunsrück, et plus globalement la géométrie du toit du socle sous le bassin. L'analyse des lignes sismiques 2D et des données de puits a permis de contraindre la structure et la formation du pli d'Alsting. La carte du toit du socle met en évidence une structuration en hauts de socle (−1, 5 km) et des zones d'approfondissement de socle (−6, 5 km) orientés NE-SW, NNE-SSW à N-S et NW-SE. Cette structuration explique les variations spatiales des épaisseurs des séries sédimentaires en place. La première dérivée verticale de l'anomalie de Bouger montre que la zone de faille de Metz-Hunsrück est continue et limite les bassins houillers lorrain et sarrois. Par ailleurs, les interprétations sismiques montrent que le pli d'Alsting est un pli-faille dont la formation et l'érosion post- compression se sont produites pendant le Stéphanien. Après cette déformation, la subsidence et de dépôt ont repris à la fin du Stéphanien. Cette étude met en évidence une histoire géologique Stéphanienne différente du bassin Lorrain par rapport aux autres bassins

Mots-clés : Bassin Houiller de Lorraine (BHL) / structure du socle du socle et du bassin / compression Stéphanienne / Zone de Faille de Metz-Hunsrück / variations d'épaisseur / formation du pli sur chevauchement d'Alsting

*Corresponding author: metzger.mombo-mouketo@univ-lorraine.fr

1 Introduction

The Westphalian coal seams of the Lorraine Coal Basin (LCB) and its prolongation in Germany known as the Saar-Nahe Coal Basin (SNCB) (Fig. 1) have been long exploited while less economical attention was paid to their methane content. Since 2015, this methane has been explored by La Française de l'Energie company (FDE). This momentum led to the creation of the REGALOR project (REssources GAzières de LORraine) that aims in part to re-evaluate the structural organization of the basin for a better characterization of this resources. After the review of the literature in the basin, the structure Metz-Hunsrück-Fault-Zone (MHFZ) and that of the basement beneath the sedimentary cover as they are still badly constrained. For that, the first vertical derivative and the top basement map are constructed from the Bouguer to highlight the geometry of both structures and understand their relationship with the total thickness variation in the basin. Furthermore, within the FDE exploration permit (located in the north-eastern part of the basin), most of the previous structural studies focused on the Merlebach (MTF), the Saarbrucken (STF) and the Pont-à-Mousson (PaMTF) thrust folds (Pruvost, 1934; Donsimoni, 1981; Pryvalov *et al.*, 2015; Beccaletto *et al.*, 2019; Hemelsdaël *et al.*, 2023) while the Alsting fold (ATF) (Fig. 2a) did not received much attention. Since it is a target for the company, deciphering its structure and its formation is useful for its exploration but also to understand the full picture of the deformation evolution in the LCB. A set of 2D seismic lines (Fig. 2a) and well data provided by la FDE are used for this purpose.

2 Geological context

2.1 The LCB-SNCB in the framework of the Variscan belt

The LCB and the SNCB form a north-east to north-north-east trending Upper Carboniferous-Permian basin that extends by 300 km long and 80 km width (Fig. 1), with almost 6–7 km of preserved strata (Donsimoni, 1981). The basin developed on the Mid German Crystalline High (MGCH) during the late variscan period due to the activity of the Metz-Hunsrück-Fault-Zone (MHFZ), which limits the basin in the north (Pruvost, 1934; Donsimoni, 1981; Anderle, 1986; Henk, 1993; Korsch and Schäfer, 1995; Schäfer, 2011). The basin is limited by other major variscan structures (Fig. 1), the La Marne fault (MaF) in the west, and the saxothuringian limit in the south (Donsimoni, 1981; Franke, 2014). The basin's development is linked to the orogenic and post-orogenic deformation evolution of the rhenohercynian and the MGCH (Donsimoni, 1981; Anderle, 1986; Henk, 1993; Korsch and Schäfer, 1995; Hemelsdaël *et al.*, 2023).

The orogenic period was marked by the convergence between the rhenohercynian unit and the MGCH during Frasnian and the Upper Carboniferous (Oncken, 1998). This convergence led to the folding and thrusting of the Devonian-Lower carboniferous marine strata deposited on the rhenohercynian unit were. From Namurian-Westphalian, the deformation propagation of the variscan front toward the north initiated the development of foreland paralic coal basins such as the Ruhr and the Namur (Fig. 1) whereas the LCB and SNCB and other limnic coal basins developed on the MGCH (Pruvost, 1934; Alpern *et al.*, 1969; Zimmerle, 1976; Donsimoni, 1981; Schäfer, 1989). Yet, from the Westphalian, the stress regime under which the LCB and SNCB developed is still debated. The geodynamic models proposed by Arthaud and Matte (1977) and Burg *et al.* (1994) which suggests a syn-orogenic extension/transtensional regime during Westphalian and a post-orogenic extension during Stephanian-Permian as largely been used to explain the basin's development (Donsimoni, 1981; Korsch and Schafer, 1995; Privalov *et al.*, 2015; Henk, 1993) and that of several other coal basins (Faure, 1995; Henk, 1993; Donsimoni, 1981; Korsch and Schäfer, 1995; Djarar *et al.*, 1996; Allemand *et al.*, 1997; Averbuch et Piromallo, 2012; McCann *et al.*, 2006). However, other authors (Anderle, 1986; Kroner *et al.*, 2008; Corsini and Rolland, 2009; Kroner and Romer, 2013; Stephan *et al.*, 2016) argued for a compressional/transpressional regime during the Namurian-Westphalian in the rhenohercynian and saxothurigian units. Anderle (1986) links the LCB and SNCB initiation to this compressional/transpressional regime.

After this compressive setting, the Late Carboniferous-Permian period was governed by extension and magmatism (Faure, 1995). In the SNCB, the volcanism is Permian and dated close to 290 Ma (Lippolt and Hess, 1989), while there is no absolute dating in the LCB (Donsimoni, 1981). During Triassic, a continental and restricted marine setting developed (Guillocheau *et al.*, 2000) over the rhenohercynian domain and the MGCH that led to the shallow burial of the LCB and SNCB Upper Carboniferous-Permian strata. During the Jurassic and the Lower Cretaceous, the LCB, the SNCB, and the southern part of the Hunsrück-Taunus formation were deeply buried under the Mesozoic formations (Guillocheau *et al.*, 2000; Prijac *et al.*, 2000; Le Solleuz *et al.*, 2004). Later during Cretaceous, the rhenohercynian domain was uplifted and a part of the SNCB underwent an erosion (Anderle, 1986; Hertle and Littke, 2000). This erosion made a part of the Upper Carboniferous formations of the SNCB outcrop (Fig. 2a).

2.2 Existing tectono-sedimentary models of the LCB and SNCB

2.2.1 The Lorraine Coal Basin (LCB)

Different structural models have been proposed for the LCB. Pruvost (1934) was a pioneer scientist that discussed the global structural evolution of the basin. Donsimoni (1981) was the first to propose that the basin developed due to the reactivation of the MHFZ as a normal fault. He summarised its tectono-sedimentary evolution into four major stages: (1) the deposition of the Namurian-Westphalian D, (2) a weakly folding phase during Late Westphalian D, (3) a renew of the subsidence and deposition during Stephanian-Permian, (4) and finally the major folding and thrusting phase during Mid-Permian. Micro-structural data measured on thrusts and on strike-slip faults in galleries suggest that the compression was oriented NW-SE (Blès and Lozes, 1980; Donsimoni, 1981). This Permian shortening phase led to the current organisation of the fold and synclines (Fig. 2b) according to the author.

Pryvalov *et al.* (2015) interpreted the LCB and the SNCB as a large pull-apart basin with a local extension-compression

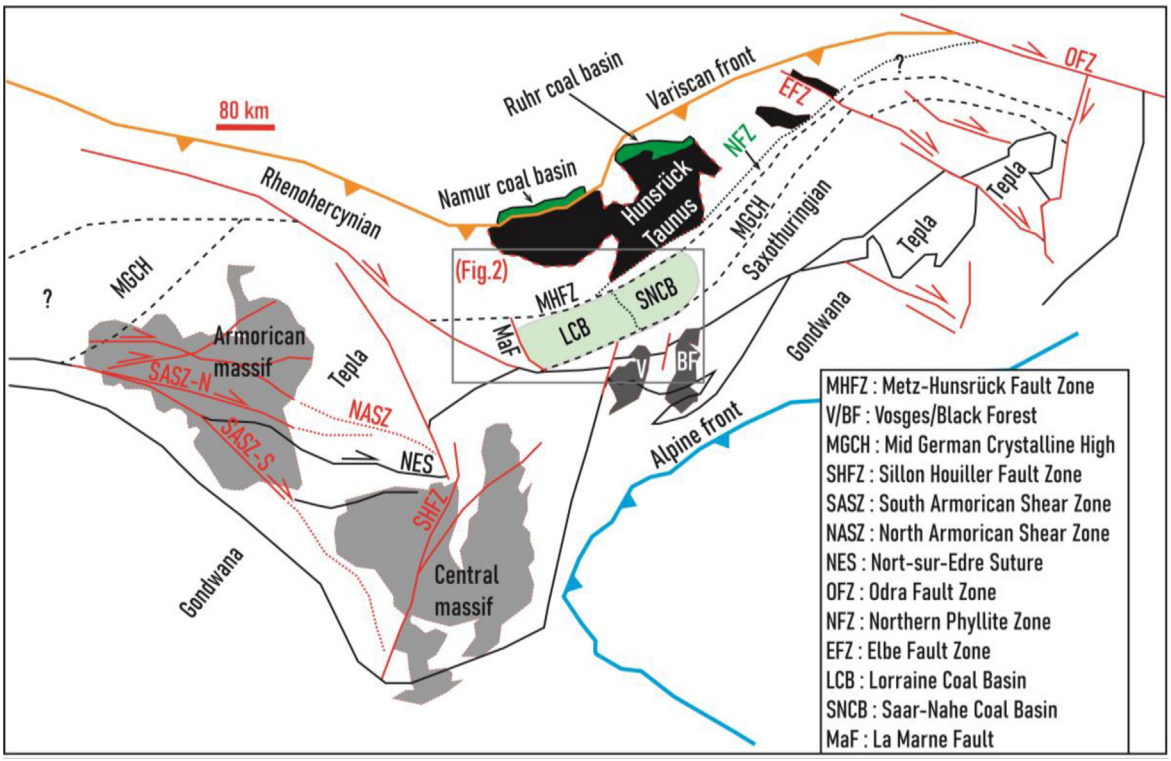

Fig. 1. The Lorraine Coal Basin (LCB) and the Saar Nahe Coal Basins (SNCB) within the Variscan orogeny units (modified from Franke, 2014).

due to the basement-block rotations. The author interpretation is based on the observation of the cleat (fractures in coal seams) geometry through the X-ray tomography without any observations at the basin scale.

More recently, Beccaletto *et al.* (2019) and Hemelsdaël *et al.* (2023) show that LCB developed as a compressive basin along the Metz thrust (a NW-dipping thrust) during the Namurian-Westphalian. In addition, their seismic interpretations highlighted Westphalian C and D growth strata involved in the PaMTF that led to infer that age of the deformation in the basin.. Furthermore, the authors highlighted syn-sedimentary normal faults that control the Stephanian strata deposition in the south-western part of the LCB (Fig. 2a). At the basin scale, the author interpret these faults as the consequence of the post-orogenic extension accommodated by the Hunsrück fault. This model suggest that the Metz-Fault and the Hunsrück Fault are two different faults.

2.2.2 The Saar Nahe Coal Basin (SNCB)

In the SNCB, three different structural models were proposed based on different interpretations of the MHFZ imaged by the DEKORP 1C-9N seismic line. Anderle (1986) interpreted the SNCB as a compressive basin from the Namurian until the Late Westphalian and which switched into an extensional one during Late Carboniferous due to the collapse of the variscan orogeny. Anderle (1986) suggested a Late Carboniferous compression for the Saarbrücken thrust-fold formation while Engel (1985) suggested a Stephanian- Permian compression. Before the well-known paper of Korsch and Schäfer (1995), the Saarbrucken thrust fold has been interpreted as a positive flower structure linked to the strike-slip motion along the MHFZ (Drozdzewski and Juch, 1992; Juch *et al.*, 1994). Korsch and Schäfer (1995) interpreted the LCB and the SNCB as a transtensional pull-apart based on the : (1) the interpretation of the MHFZ as a steep fault, (2) the north-eastward depocenter migration from the LCB to the SCB deduced from thickness maps from well data and (3) the subsidence curve which is like those of strike-slip basins.

Henk (1993) on the contrary, interpreted the MHFZ as a detachment fault. The author proposed that the SNCB developed as a compressive basin until Westphalian B and which became an extensional basin due to the E-W extension from Westphalian C. In this model, the extensional reactivation of the MHFZ leads to the collapse and segmentation of the MGCH basement into sub-blocs separated by first order NW-SE right-lateral transtensional faults (Fig. 2a). These NW-SE first-order faults created sub-basins separating the LCB with the SNCB. This collapse led to the formation of the Saarbrucken thrust fold according to Henk (1993). Such first order transfer faults have never been clearly observed on seismic data. However, the second and third order NW-SE, and E-W strike-slip faults (Fig. 2a) segmenting the LCB-SNCB into small horsts and grabens have been proved (Engel, 1985; Stollhofen, 1998; Juch *et al.*, 1994; Becker and Schäfer, 2020, 2021).

2.3 Lithostratigraphy of the LCB

Two Upper Carboniferous stratigraphic sub-stages (Fig. 3) have been defined in the LCB and the SNCB based on paleontological studies (Bertrand, 1928; Pruvost, 1934; Laveine, 1974; Kelch and Reible, 1976), palynology (Alpern *et al.*, 1969) and on of well-known tonstein layers (Termier, 1923; Pruvost, 1934; Merry, 1967; Lippolt and Hess, 1989;

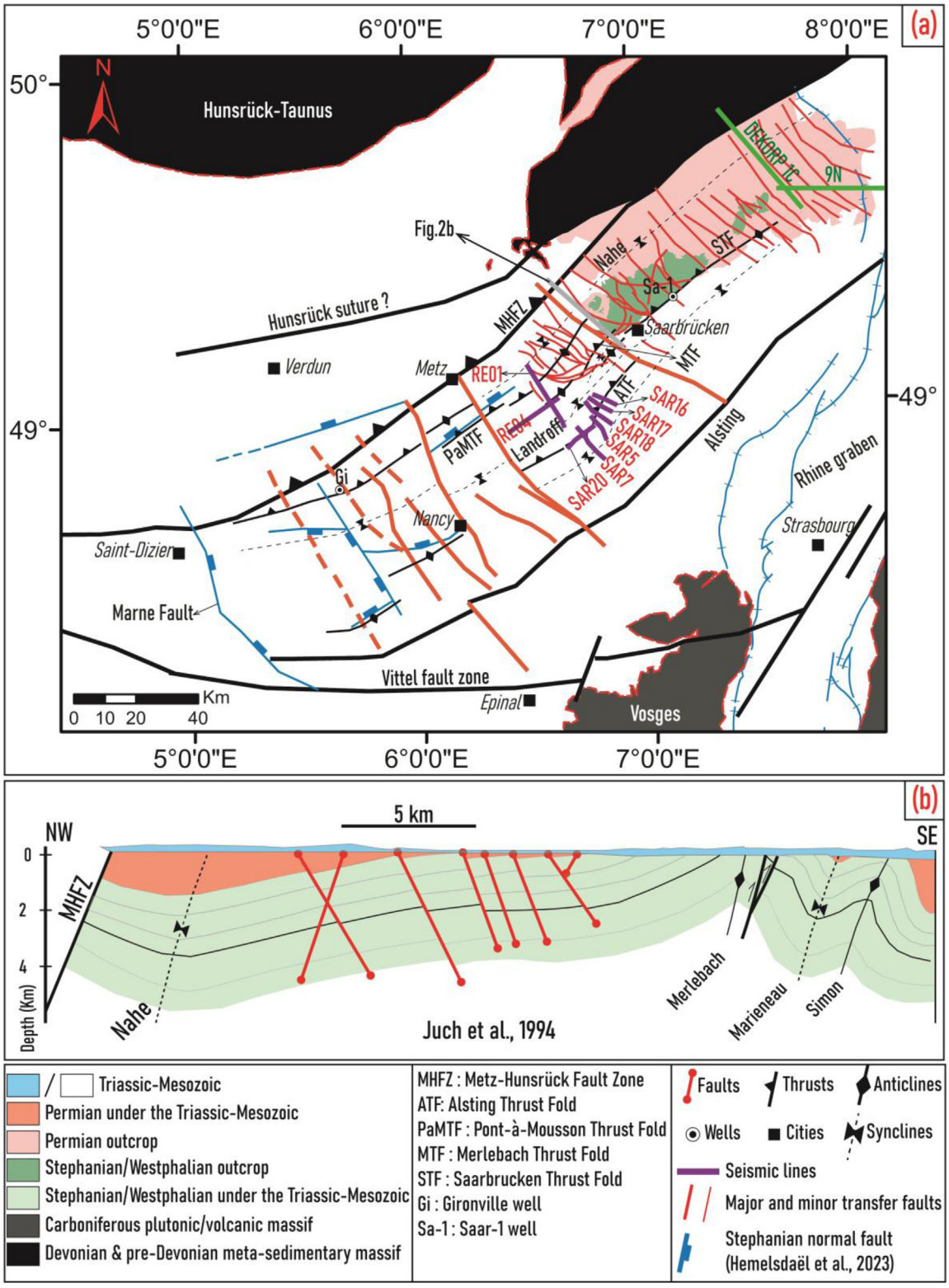

Fig. 2. (a) Structural map of the LCB-SNCB (modified from Pruvost, 1934; Hannover, 1979; Donsimoni, 1981; Stollhofen, 1998; Hemelsdaël *et al.*, 2023). The map is projected using the Lambert 93 system. (b) A Cross-section (grey line on (a)) at the France-Germany boundary showing the current geometry of the thrust-folds (modified from Juch *et al.*, 1994).

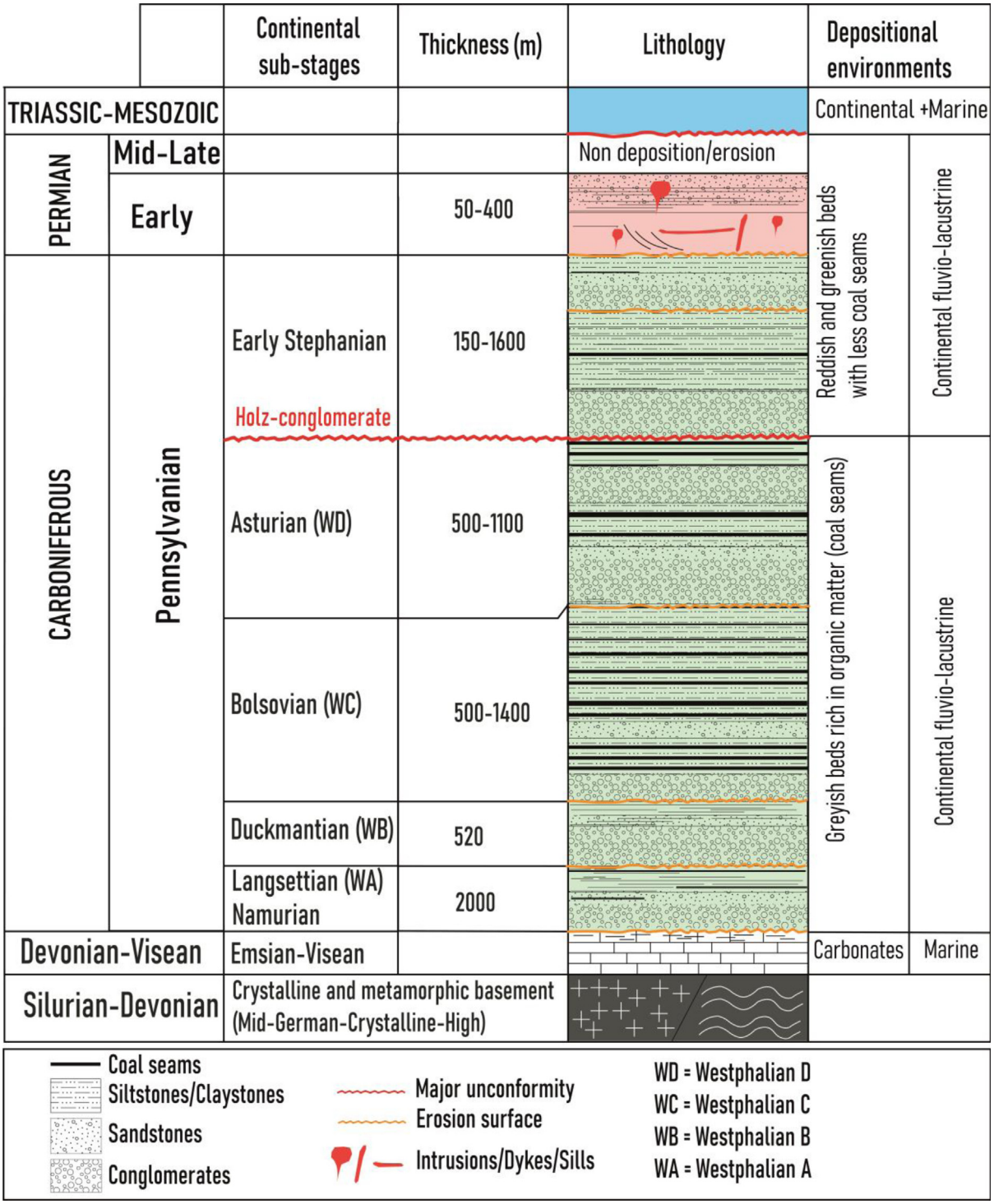

Fig. 3. Lithostratigraphy of the LCB with the different sub-stages defined in the Westphalian and Stephanian (modified from Donsimoni, 1981).

Burger *et al.*, 1997; Königer *et al.*, 2002). The Namurian-Westphalian, the oldest interval, consists of almost 4 km of finning upward sequences of conglomerates, sandstones with intercalated siltstones/claystones, and multiple coal seams. These sequences deposited in alluvial, braided, meandering fluvial, floodplain or swamps, and lacustrine environments (Donsimoni, 1981; Schäfer, 1989; Izart *et al.*, 2005). The petrographic components of the Westphalian sandstones and conglomerates suggest that the Rhenohercynian metamorphic and sedimentary massif was the principal sediment source (Pruvost, 1934; Schäfer, 2011). The Westphalian was subdivided into Westphalian A, B, C, and D sub-stages based on plant distribution. These continental sub-stages correspond respectively to the Langsettian, Duckmantian, Bolsovian, and Asturian (Aretz *et al.*, 2020). Izart et al (2025) have just published the first absolute dates in the BHL. These confirmed

the stratigraphic age of tonstein T600 (Duckmantian-Bolsovian boundary), from tonsteins T10 to the top of the Asturian. The continental nomenclature will be preferred in this study to ensure consistency between well data lithostratigraphy and seismic horizon interpretation.

The second sub-stage recognized is the Stephanian, whose basis is represented by the Holz conglomerate formation (Fig. 3), which is often discordant with the underlying Westphalian. In the LCB, only the Early Stephanian is known (Alpern *et al.*, 1969) while the entire Stephanian is recognized in the SNCB (Schäfer, 2011). Izart *et al.* (2025) dated the other tuffs and constrained the hiatus below the Holz conglomerate, which corresponds to 2 Ma. This hiatus corresponds to the Lower and Middle Cantabrian stage (Izart *et al.*, 2025) and is due to the post-folding erosion (Pruvost, 1934; Donsimoni, 1981; Hemelsdaël *et al.*, 2023). Absolute dates are also available for the SNCB from several studies (Burger *et al.*, 1997; Königer *et al.*, 2002; Königer and Lorenz, 2002; Menning and Bachtadse, 2012; Voigt *et al.*, 2022). According to Schäfer (1989), the richness in feldspars and the change of the paleo-current sense suggest that the sediment was supplied by the granitic massifs in the south.

Both formations are overlain by the Lower Permian continental red sediments, which are heterogeneously recognised in both basins (Schäfer, 2011). The two sub-stages (Lower Rotliegend equivalent to Autunian and the Upper Rotliegend) are recognised in the SNCB while only the Saxonian facies, equivalent to a part of the Upper Rotliegend has been recognised in the LCB (Donsimoni, 1981). In the LCB, this Saxonian facies can easily reach 700 m of thickness (Donsimoni, 1981) and is composed of continental red conglomerates, sandstones, and claystone, deposited in alluvial, fluvial, and lacustrine environments (Donsimoni, 1981; Schäfer, 2011). Furthermore, several magmatic intrusions and sills (basaltic, andesitic, and rhyolitic intrusions and sills) affected SLB during the Early Permian (Lippolt and Hess, 1989). In the LCB, the volcanic bodies have been mapped using seismic, gravity and well data, but have never been dated (Donsimoni, 1981; Hemelsdaël *et al.*, 2023).

3 Dataset

Dataset used in this study comprises a network of 2D seismic lines (Fig. 2a), mining and petroleum wells (Fig. 4a), and gravity data which are detailed in the following sections.

3.1 Well data

Figure 4a presents the location of all the wells used in this study. Most of the wells named SJ prefix have been drilled by the HBL (Houillère du Bassin Lorrain) company during the mining explorations to characterize the coal seams. They possess a very detailed description of the facies, the different tuffs layers (tonsteins), and the palynology of the different units crossed, allowing to identify the different Carboniferous sub-stages limits. These wells can be freely downloaded (infoterre[1]). The rest of the wells were drilled during the exploration of hydrocarbons and possess logging data, and the different stratigraphic stages and sub-stages limits were determined by palynology as well.

3.2 Gravity data

The Complete Bouguer Anomaly data (CBA) used covers the LCB, the SNCB, and their surrounding basement units. The data is part of the work of the AlpArray Gravity Research Group (AAGRG) (Zahorec *et al.*, 2021). The CBA was corrected using an average density of 2,670 kg m^{-3}, and the terrain corrections were made with different DEM (Digital Elevation Model) of different resolutions, ranging 5 m to 30 m (see Zahorec *et al.*, 2021 for more details). To map the geometry of the MHF, the First Vertical Derivative (FVD) of the residual Bouguer anomalies was computed to enhance the anomalies for better interpretation (Fig. 5). The map top basement map (Fig. 6) is generated through the application of the Source Parameter Imaging Method (Thurston and Smith, 1997; Smith *et al.*, 1998; Essa *et al.*, 2022). Furthermore, a spectral analysis was applied on the Bouguer anomaly. This allows to identify the depth of the different gravity anomalies and to separate the regional from the residual anomalies (Spector and Grant, 1970; Essa *et al.*, 2018; Mazur *et al.*, 2020; Ganguli *et al.*, 2020).

3.3 Seismic-to-well tie

The eight seismic lines presented in this study are located in the north-east part of the LCB (Fig. 2a) and were provided by "Française de l'Energie" (FDE) company. They comprise six post stacked migrated seismic lines (SAR5, SAR7, SAR16, SAR17, SAR18, and SAR20) acquired in 1989 and two vintage seismic lines (RE01 and RE04) acquired in 1958. Amplitude corrections (AGC: Amplitude Gain Correction), DMO (Dip-Move-Out) correction and post-stack migration were applied to the SAR lines by the FDE. The vintage lines were depthmigrated using linear velocities laws. No further information is available about this time-to-depth conversion. Their quality is poorer compared to the SAR lines. The Seismigraphix[2] open-source software was used to display the 6 SEG-Y seismic lines in order to obtain a high resolution images and their interpretation were done in Adobe Illustrator 2019.

The seismic-to-well-tie method does not rely on check-shot since they are not available on the wells located in our study area. However, the sonic log was used to convert the top of each Carboniferous sequence crossed by the Vaxy (Va), Morhange (Mo-1) and Germisay (L.Ge-1) well into time by using the sonic velocities of conglomerate, sandstones, claystones and coals, and the percentages of facies in each carboniferous sequence (Fig. 4b). This time was compared with the interpreted limit of each formation in the seismic lines. The intersections between these seismic lines allowed us to know the time of each formation in all the seismic sections.

4 Results and interpretations

4.1 Basement structuration

4.1.1 The structure of the gravity anomalies

Figure 5 presents the interpretations of the first vertical derivative which shows that the rhenohercynian unit, the LCB and

[1] https://github.com/abelsurace/seismigraphix

[2] https://infoterre.brgm.fr/viewer/MainTileForward.do

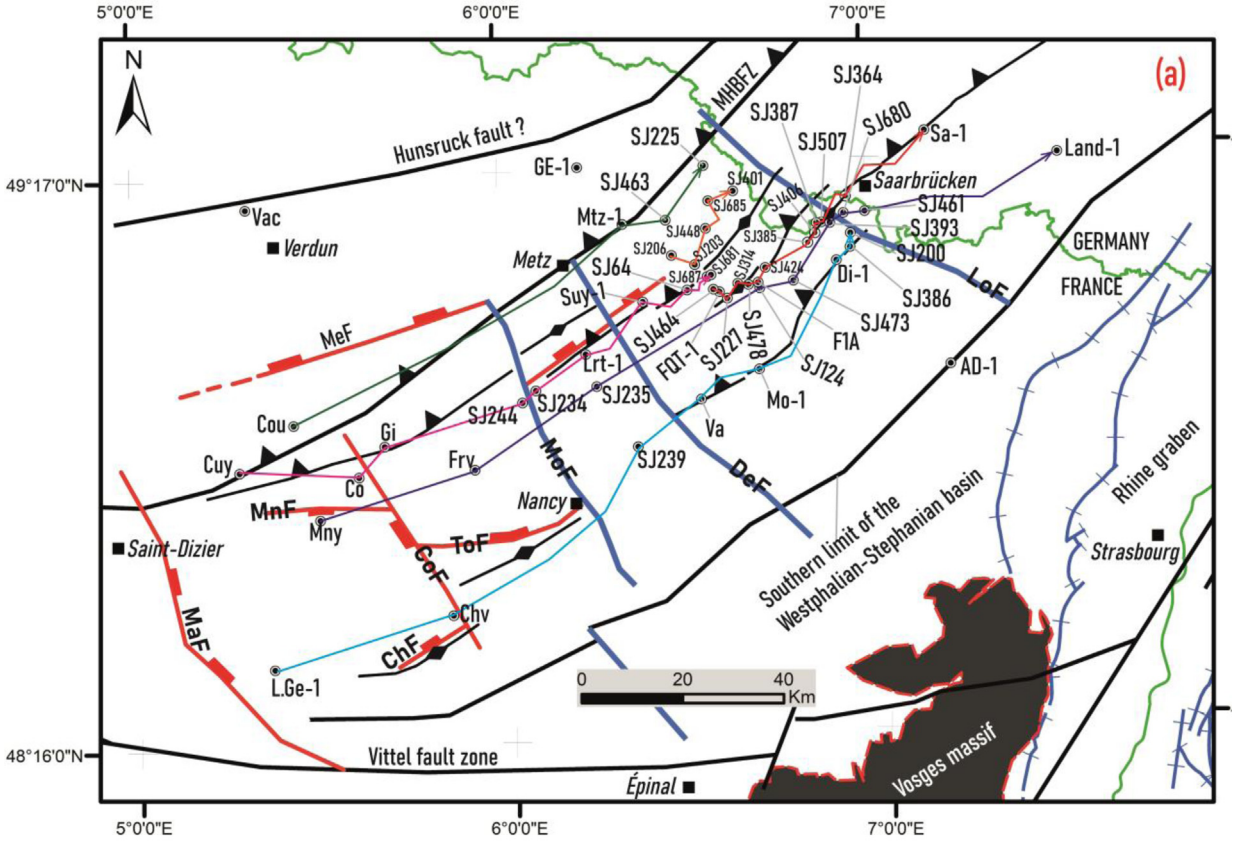

Data	Facies % on each well	Base Depth (m)	Sonic velocities (m/s)	Time (s) after sonic	Time (s) on seismic lines
Stages/ Borehole	Vaxy	Vaxy	Vaxy	Vaxy	Vaxy (LOR 09) (b)
Mesozoic	Cg(6)+Sa(43)+Cl (31)+Li (20)	800	2462	0.65	0.65
Permian	Sa(50)+Cl(50)	901	4040	0.7	0.7
Stephanian	Cg(5)+Sa(44)+Cl (43)+Co(8)	1001	4000	0.75	0.75
Westphalian D	Cg(1)+Sa(20)+Cl (73)+Co(6)	1652	3946	1.08	1.08
Stage / Borehole	Morhange	Morhange	Morhange	Morhange	Morhange (SAR20 and SAR1)
Mesozoic	Cg(7)+Sa(48)+Cl (26)+Li (19)	799	2663	0.6	0.6
Permian	Sa(75)+Cl (25)	1055	5120	0.7	0.7
Stephanian	Cg(2)+Sa(73)+Cl (25)	2268	4411	1.25	1.25
Westphalian D	Cg(6)+Sa(41)+Cl (48)+Co(5)	3000	4182	1.6	1.7
Stages/ Borehole	Germisay	Germisay	Germisay	Germisay	Intersection TOUL 12 /TOUL10
Mesozoic	Sa(20)+Cl (40)+Li (40)	1429	3572	0.8	0.8
Permian	Cg(30)+Sa(20)+Cl (50)	3429 (2757)	3400	2	2
Stephanian	Sa(60)+Cl (40)	6429	4000	3.5	3.5

Fig. 4. (a): Wells location on the structural map. Note also the location of the different NE-SW sub-stages thickness profiles from well data. These thickness profiles are presented on Figure. The map is projected with Lambert 93 system explaining the gap of the X and Y coordinates locations. (b): Summary of the different parameters used in the seismic-to-well tie procedure. Cg (conglomerate), Cl (claystone), Co (coal), Li (limestone) and Sa (sandstone).

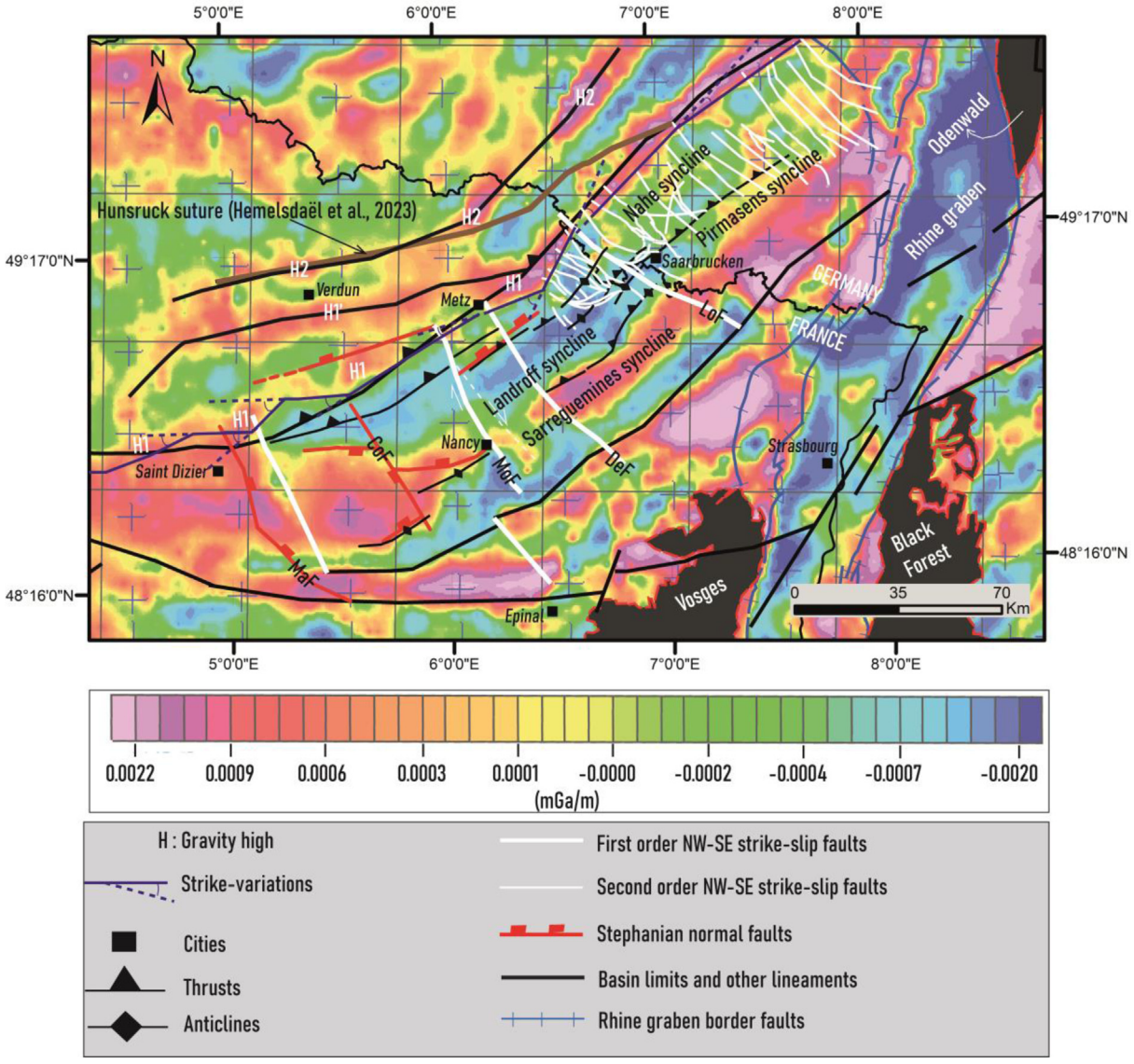

Fig. 5. Map of the first vertical derivative highlighting the geometry of the MHFZ. Note the different abrupt changes of the MHFZ orientation from the SNCB to the LCB. The map is projected with the Lambert 93 system. The vertical and horizontal represent the grid used to compute the map and not the longitude and latitude lines. The later are represented by the cross visible on the map.

the SNCB, and the Vosges-Black domains are structured by an alternation between NE-SW trending gravity highs (warm colours) and gravity deeps (blue areas) (Fig. 5) consistent with the orientation of the major Variscan basement lineaments in the area (Edel and Schulmann, 2009). The most interesting gravity highs are the H1, H1' and the H2 in the rhenohercynian area (Fig. 5). In detail, the H1 is a continuous lineament from the SNCB (where the MHFZ crops out) until the Metz city in the LCB (Fig. 5). Then it becomes discontinuous and less straight from the Metz to the South-Western part of the LCB where it is buried under the Mesozoic-Triassic and the Stephanian-Permian strata. In addition, the MHFZ shows strike changes from the SNCB until the LCB. The significance of all these anomalies is discussed further.

4.1.2 The basement top structure

The basement here are the MGCH and the Devonian-Mississippian metasedimentary formations beneath the LCB and the SNCB. Unlike the well data, the overall map of the basement top (Fig. 6) allows to have a continuous picture of the global thickness variations of the sedimentary cover. A comparative analysis was conducted using this map and the wells which reach the basement. For the Gironville (Gi) well, the top basement is at 5.6 km of depth, and our estimation from gravimetric data predicts 5.6 km of depth, showcasing a good agreement. However, for the Saarbrücken (Sa-1) well in the SNCB, the recorded depth of the basement top is around 5.6 km, which does not fit with the corresponding computed values around 4.6 km.

Nevertheless, this map highlights a complex geometry of the basement top with the presence of highs (1.5 − 3 km) and deeps (>4 km) of different sizes, geometries and orientations. Regarding the deeps, the NE-SW and the NNW-SSE are the dominant structures. The NE-SW deeps align with the major synclines (Landroff, Pirmasens and the Sarreguemines) in both

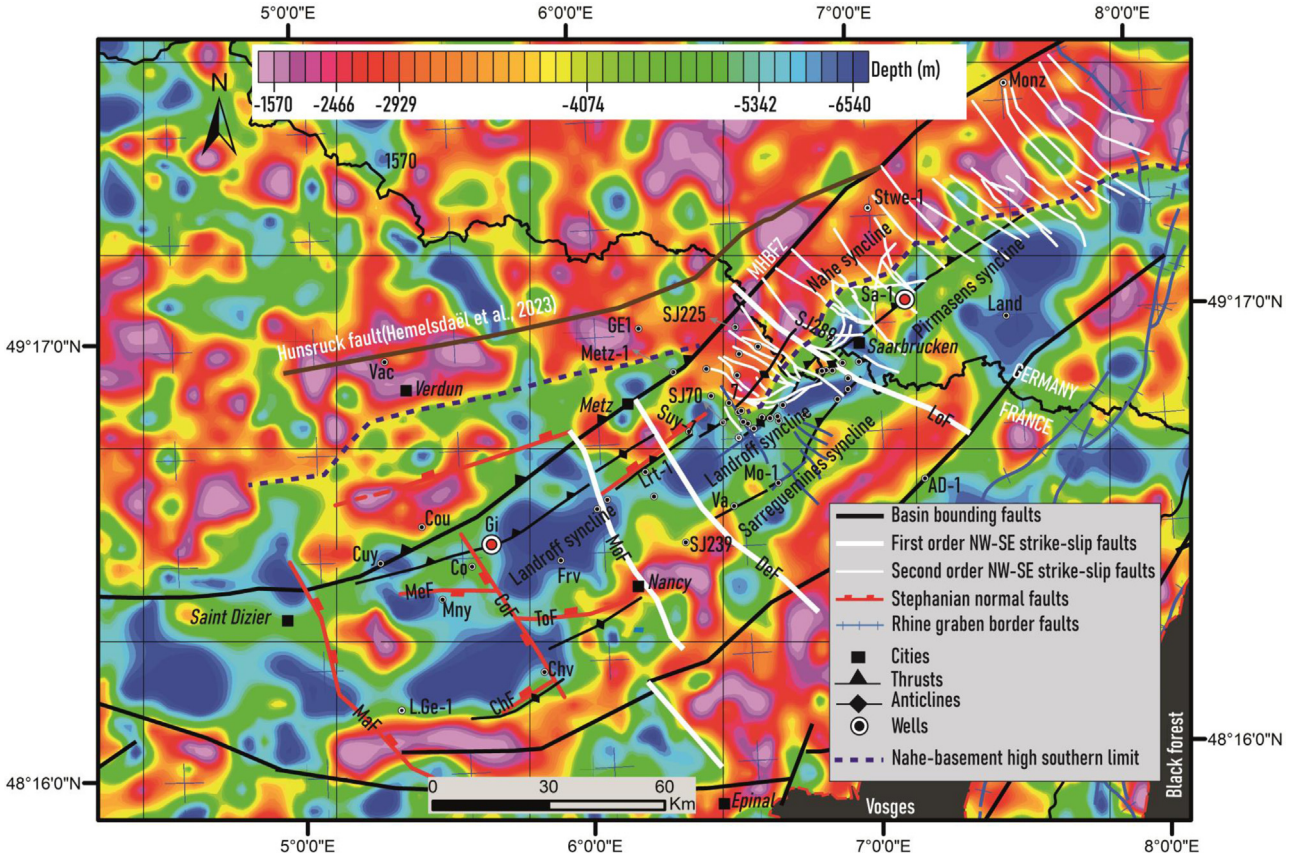

Fig. 6. Map of the top of the basement under the LCB and the SNCB highlighting the presence of basement highs and throughs of different geometries, orientations and lengths. The map is projected with the Lambert 93 system. The vertical and horizontal represent the grid used to compute the map and not the longitude and latitude lines. The longitude and latitude lines are represented by the cross visible on the map. The Gironville (Gi) and the Saar-1 (Sa-1) wells that reach the basement are highlighted with bigger circles.

basins except in the SNCB where map shows a large basement high highlighted by the violet dash-line in the Nahe-syncline (Fig. 6). The deeps length varies between 10 and 50 km and their width between 5 and 20 km. Some of the NW-SE deeps align with the NW-SE faults (Fig. 6). Their length varies between 10 and 30 km and their width between 5 and 10 km (Fig. 6). Regarding the deeps, the deep located in the Nahe-syncline is the largest with 130 km of length and a width varies from 20 to 40 km (Fig. 6). The other deeps are located at the LCB south basin borders, below the city of Nancy, around the Courcelles (Cou) well, and near the MAF fault. The significance of all these structures is discussed further.

4.2 Basin structuration

4.2.1 Sedimentary thickness from wells

Figure 7 gives important insights on the thickness variations, particularly for the Triassic-Mesozoic, the Permian, and the Stephanian sequences which are entirely crossed by many wells. The first striking observation is the less important thickness of the Triassic-Mesozoic sequence toward the north-east of the LCB along all the well profiles. The second interesting observation in the north-eastern part of the LCB is that the Permian and Stephanian sequences are thinner to absent at the fold hinge but thicker in the Landroff and Sarreguemines synclines. The Permian sequence thickness at the anticline crest is about 50 to 150 m while it is two or three times thicker (300−400 m) in syncline position. Likewise, the Stephanian sequence is thinner (100–200 m) to be absent in the anticline crest (SJ234, LRT-1, SUY-1, SJ64, SJ424, SJ680, and SJ393) while it is thicker (500 m−1.2 km) in the syncline. There is an exception for some wells (SJ239; Mo-1; SJ386; SJ244; SJ681; and the SJ385) located at anticline crests and which show thicker Permian and Stephanian formations. Nevertheless, all these observations suggest a close relationship between the folds and the spatial thickness variations of the Stephanian-Permian sequences.

In the south-western apart of the LCB, the wells highlight the same tendency but with a thicker Stephanian and Permian (1−2 km) compared to the thickness range observed in the north-eastern part. The thicker Permian is encountered on Germisay well (L.Ge-1), Chevraumont (Chv), Commercy (Co) wells. In the SNCB, the Land-1 and AD-1 wells, located in the Pirmasens and the southern limit of the LCB-SNCB basin show a similar range of thickness. For the Westphalian D, C, and B sequences, is it very difficult to identify a relationship with the anticline and syncline since their thickness are not entirely crossed by the different wells. The last interesting characteristic highlighted by these wells is the presence of the basement at shallow depth (800 m−1.6 km) in the northern limit of the LCB.

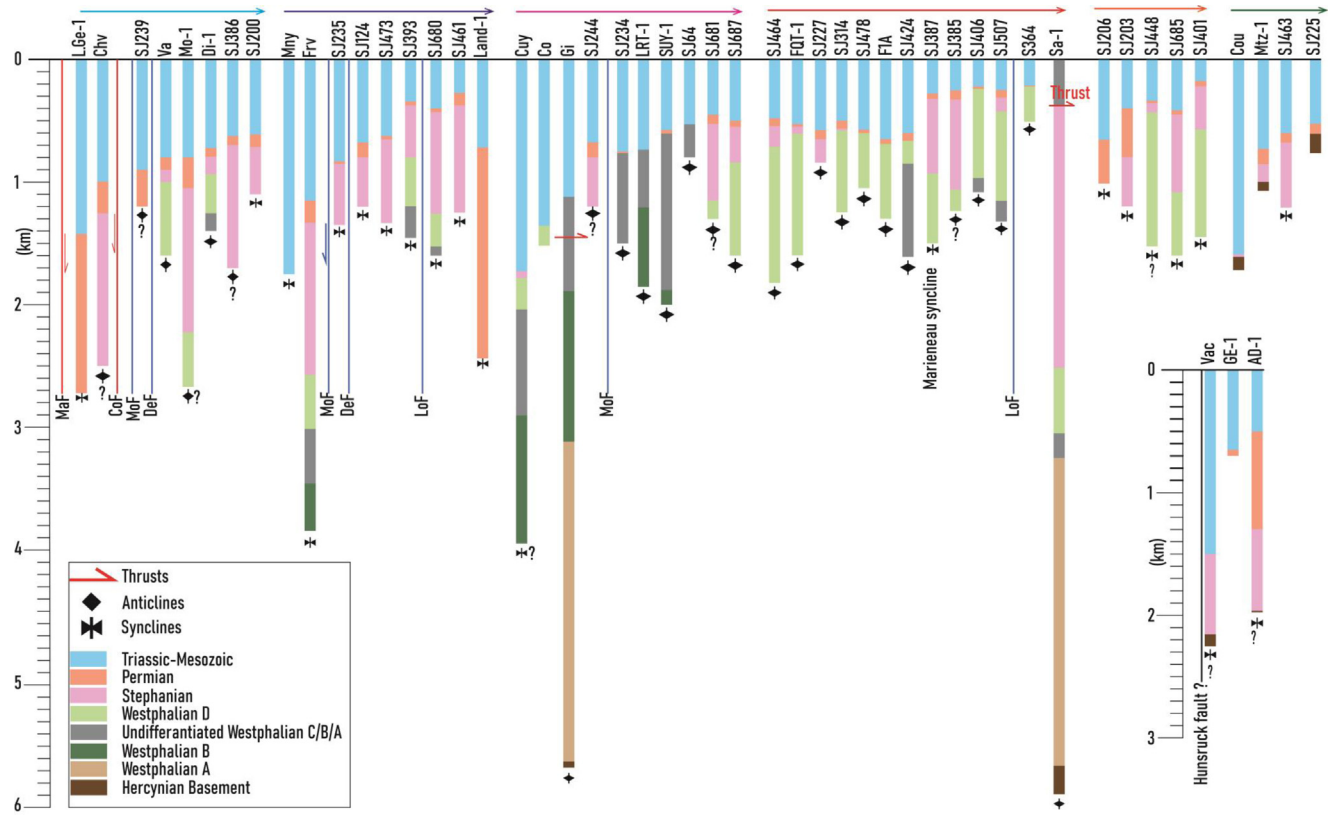

Fig. 7. NE-SW well stratigraphy profiles in the LCB-SNCB highlighting the Mesozoic thickening toward the south-west, the Permian and the Stephanian thickening in syncline and their thinning or absence in the fold hinge areas.

4.2.2 Structure of the Alsting and the Merlebach anticlines

4.2.2.1 Seismic stratigraphy

Four stratigraphic sequences have been depicted on seismic lines (Figs. 8–10) based on the time-depth presented on Figure 4b: they are the Triassic-Mesozoic, the Permian, the Early Stephanian, the Westphalian and the basement. The top basement located between 2.6–3.1 s (twt) is composed of continuous reflections in the uppermost part while the lower part is badly imaged and represented by the multiples of the upper part reflections (Figs. 8–10). The SAR07 line (Fig. 10a) highlights the shallowing of its reflections, from 3, 1s in the north-west and reaching 2.6 s (twt) toward the south-east.

The Westphalian is divided into the Westphalian D and the Undifferentiated Westphalian C/B/A separated by the Top Westphalian C limit (TWC) (Figs. 8–10). Both sub-sequences are composed of folded and thrusted reflections. These reflections are affected by erosion in the anticline crest. In detail, they consist of an alternation between low and high-amplitude and continuous reflections, which correspond to an alternation between coal seams and conglomerates and sandstones (Izart *et al.*, 2005). The Early Stephanian sequence rest conformably on the underlying Westphalian strata, implying a non-interrupted sedimentation. This allows to define the CSB as the Conformable Stephanian Basis (Figs. 8–10). Moreover, the Intra-Stephanian Unconformity (ISU) is defined within the Early Stephanian formations, separating a folded Stephanian sub-sequence with a non-folded upper sub-sequence. The upper sub-sequence is composed of reflections that fill the syncline and thin toward the hinge while the lower sub-sequence reflections are folded and thrusted.

Under the Mesozoic-Triassic formations, the Permian sequence is composed of horizontal and non-folded reflections which fill the piggyback and frontal synclines. The Permian Basis (PB) is often an irregular surface and sometimes truncates the underlying Stephanian-Westphalian, showing an erosion before the Permian deposition. This is the case at the Merlebach hinge (Fig. 11).

The Triassic-Mesozoic sequence is composed of an alternation between low and high-amplitude continuous reflections (Figs. 8–10). The Triassic-Mesozoic Basis (TMB) can be flat or irregular, and all the reflections drape the underlying Permian-Pennsylvanian strata. Furthermore, these reflections are affected by normal faults and gently folded at the location of the thrust fold hinge (Fig. 11).

4.2.2.2 The Alsting anticline

The Alsting anticline is imaged by the SAR 5, 7, 16, 17, and 18 (Figs. 8, 9, and 10b) which are perpendicular to the fold but also by the SAR20 (Fig. 10b) which is parallel to the fold strike. The SAR 5, 7, 16, 17, and 18 show that the Westphalian sequences (Westphalian D/C/B/A) are folded and thrusted by a NW-dipping fault which soles out around within the Westphalian sequence at 2.5 s (twt). Furthermore, there is no thickening of the Westphalian strata along the thrust, neither any visible preserved normal throw. In the piggyback syncline

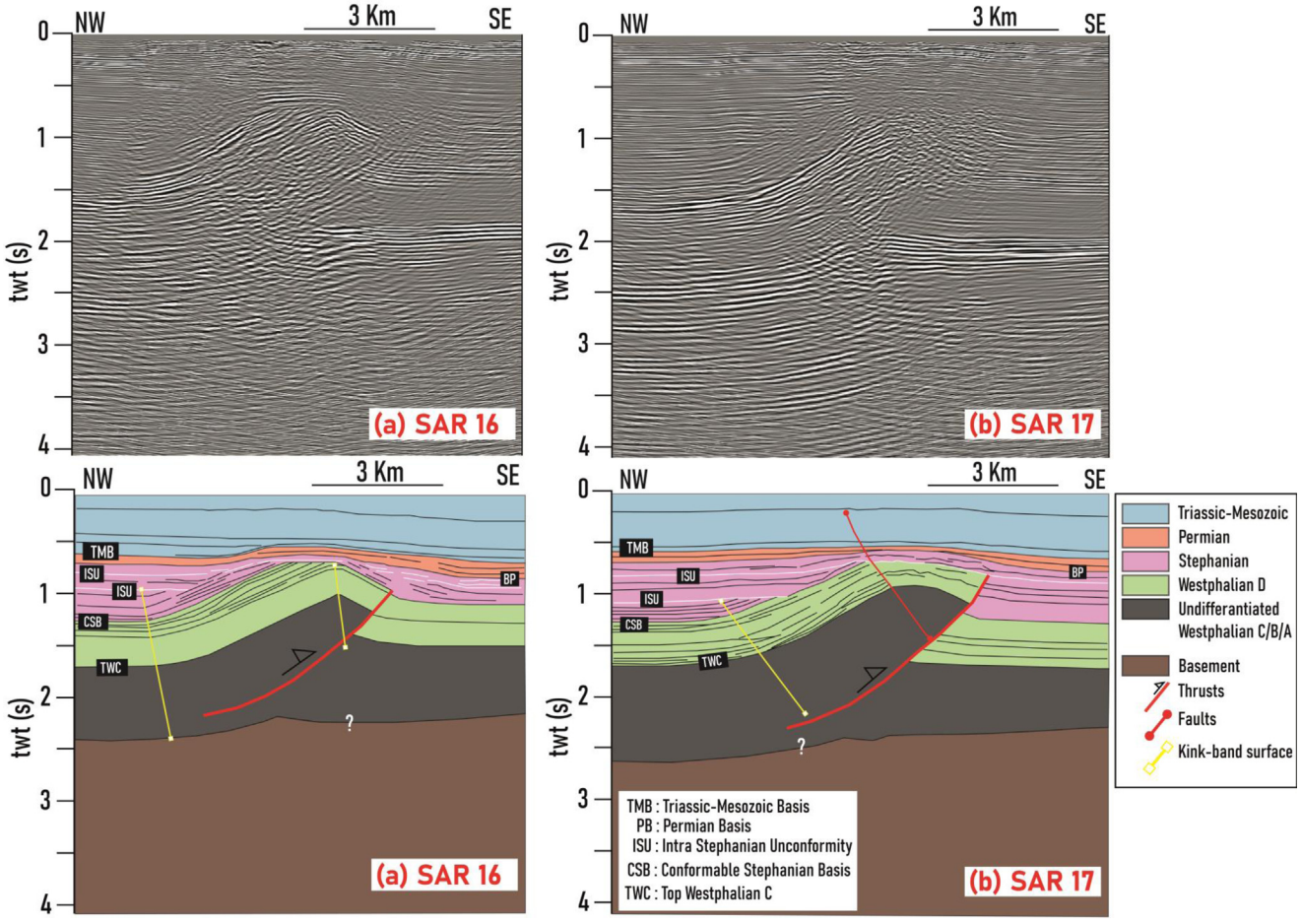

Fig. 8. (a) Uninterpreted and interpreted SAR16. (b) Uninterpreted and interpreted SAR17. These two lines highlight the structure of the Alsting anticline as a SE-vergent fault-propagation fold. Furthermore, note the presence of the ISU in the Stephanian sequence, separating a folded Early Stephanian sub-sequence with the non-folded sub-sequence. The ISU truncates the Westphalian D-Stephanian on the fold hinge.

(the Landroff syncline), the ISU separates a lower sub-sequence made up of folded strata with an upper sub-sequence made up of horizontal strata. However, on SAR20, the transition zone between the Alsting and the Morhange shows these Stephanian reflections overlaying the ISU with a fan-shape geometry.

4.2.2.3 The Merlebach anticline

The Merlebach anticline is imaged by the RE 01crossline and the RE 04 strike line (Figs. 11a and 11b). The RE 01 (Fig. 11a) highlight the anticline as an open thrust fold, with the thrust dipping toward the NW and affecting both the Westphalian sequence and the lower Stephanian sub-sequence under the ISU. Yet, the back limb of the thrust fold is very difficult to interpret due to the low quality of the line. More importantly, the line shows the strong bending of the Westphalian strata in the Landroff syncline and a thick (2 km) Lower Stephanian sequence over the ISU. In the Merlebach back limb (Fig. 11b), the RE 04 line highlights the presence of NW-SE normal faults that develop in the Lower Stephanian under the ISU.

5 Discussion

5.1 The structure of the Metz-Hunsrück Fault Zone (MHFZ)

This part discusses the structural and geological significance of the different gravity anomalies highlighted on Figure 5. If we compare the position of the gravity highs and deeps in the rhenohercynian domain with its cross-section from Oncken *et al.* (1999), it appears that the gravity deeps correspond respectively to the folded and thrust Devonian metasedimentary of the Hunsrück Nappe and the Mosel synclinoriums. Regarding the gravity highs, the H1 corresponds to the MHFZ, the H1'might correspond to a secondary fault zone that branches to the MHFZ, and the H2 is probably the Boppard thrust system zone and not the Hunsruck suture as proposed by Hemelsdaël *et al.* (2023). The gravity highs might then be interpreted as the signature of the pre-Devonian basement rocks that are involved in these thrusts' zones.

Furthermore, Figure 5 highlights almost a general strike change of theses highs and deeps toward the south-west, where

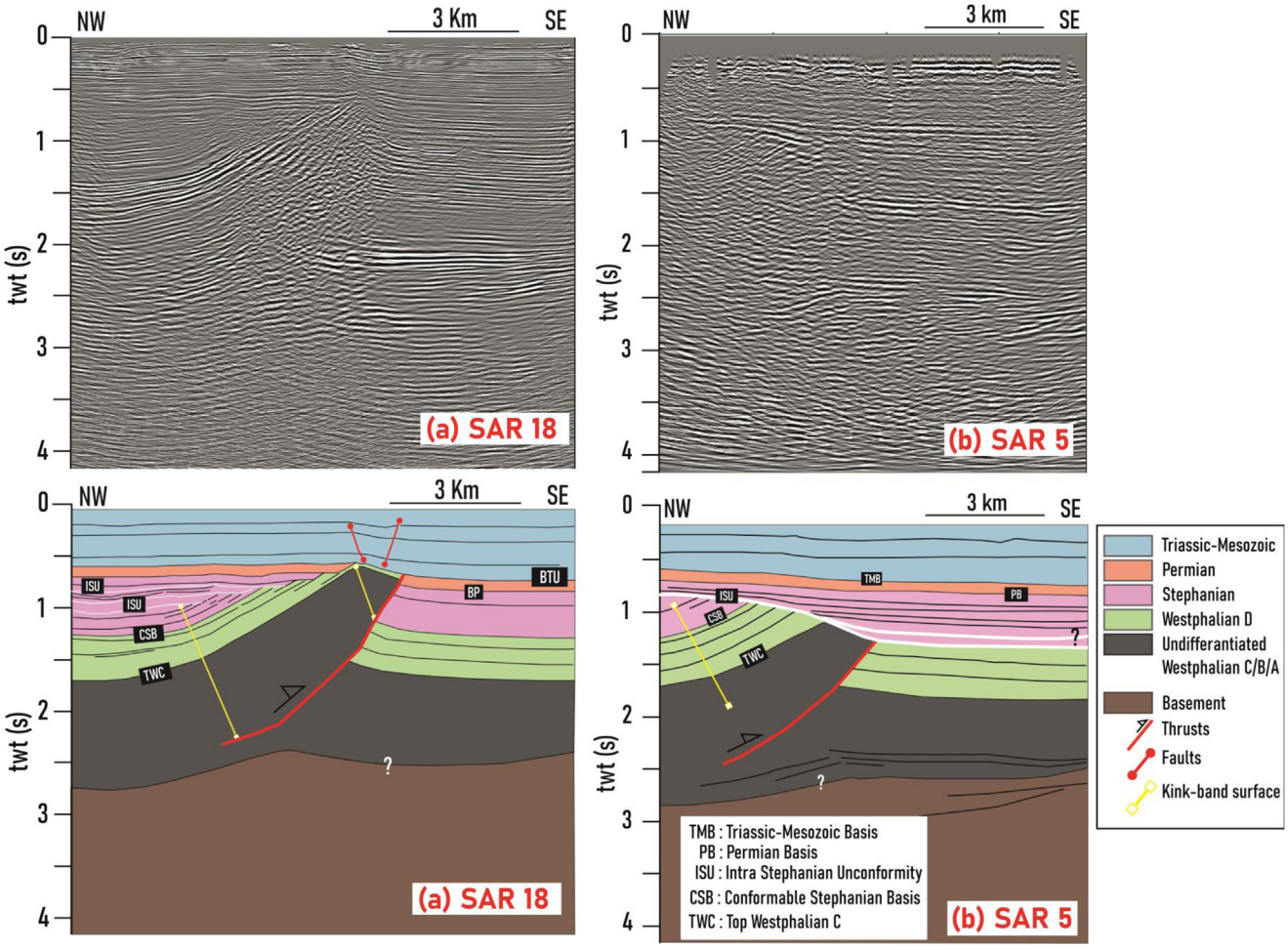

Fig. 9. (a) Uninterpreted and interpreted migrated SAR18. (b) Uninterpreted and interpreted migrated SAR5. The SAR18 highlights the same geometry observed on SAR16 and SAR17. The SAR5 line shows the ISU as a major intra-Stephanian post-folding erosion surface.

they almost become E-W tending anomalies. These data show that the MHFZ is a complex fault zone than previously thought.

Within the LCB and the SNCB, Edel and Schulmann (2009) interpreted the gravity deeps in the LCB and SNCB as the signature of a crystalline ridge (the MGCH granite/metagranite) and the gravity high in the Sarreguemines syncline as the Morhange thrust zone and the Teplà-suture zone. Finally, the gravity highs and deeps are linked to the basement structures, and the sedimentary cover effect seems to be insignificant.

5.2 Tectonic structures and sediment thickness

5.2.1 The basement highs and deeps

The depth derived with the basement top map fit very well with the depth encountered on Gironville well and Land-1 well but not for some areas or wells as it is the case of the Sa-1 well, and the depth estimated in the Nahe syncline. Therefore, the significance of these basement highs and deeps must be discussed.

The first interesting feature to discuss is the basement high which correspond to the Nahe syncline and its prolongation in the LCB. This high suggests a sedimentary thickness less than 4 km while Korsch and Schäfer (1995) and Schäfer (2011) cross-sections suggest more than 7 km. Yet, the Saint-Wendel (Stwe-1) and the Monzingen (Monz) wells drilled on this basement high only cross the Permian strata until 2 km (Fig. 3, Schäfer, 2011). Similarly to the SNCB, the SJ206, and the SJ203 in the LCB cross a thicker Permian (625 m) and reaches the Stephanian at 1.2 km (Fig. 6). All these well data therefore cannot help to be sure of the depth of the top basement predicted by our algorithm nor that suggested by the previous authors. However, the cross-section of Hannover (1979) on the Figure 3 from Izart *et al.* (2016) supports the presence of the Devonian formations belonging to the rhenohercynian unit between 1.5 and 3 km under a thick Permian and a thin Stephanian sequence, fitting with our basement high. In this case, the southern limit of the high might correspond to the Metz-Taunus Fault sensu Hannover (1979). This shows ha the MHF zone is a very complex fault zone with several fault secondary faults connecting to one another. The other explanation of this basement high could be linked to the presence of several volcanic bodies in the Nahe syncline (Schäfer, 2011). These volcanic bodies are elongated and are

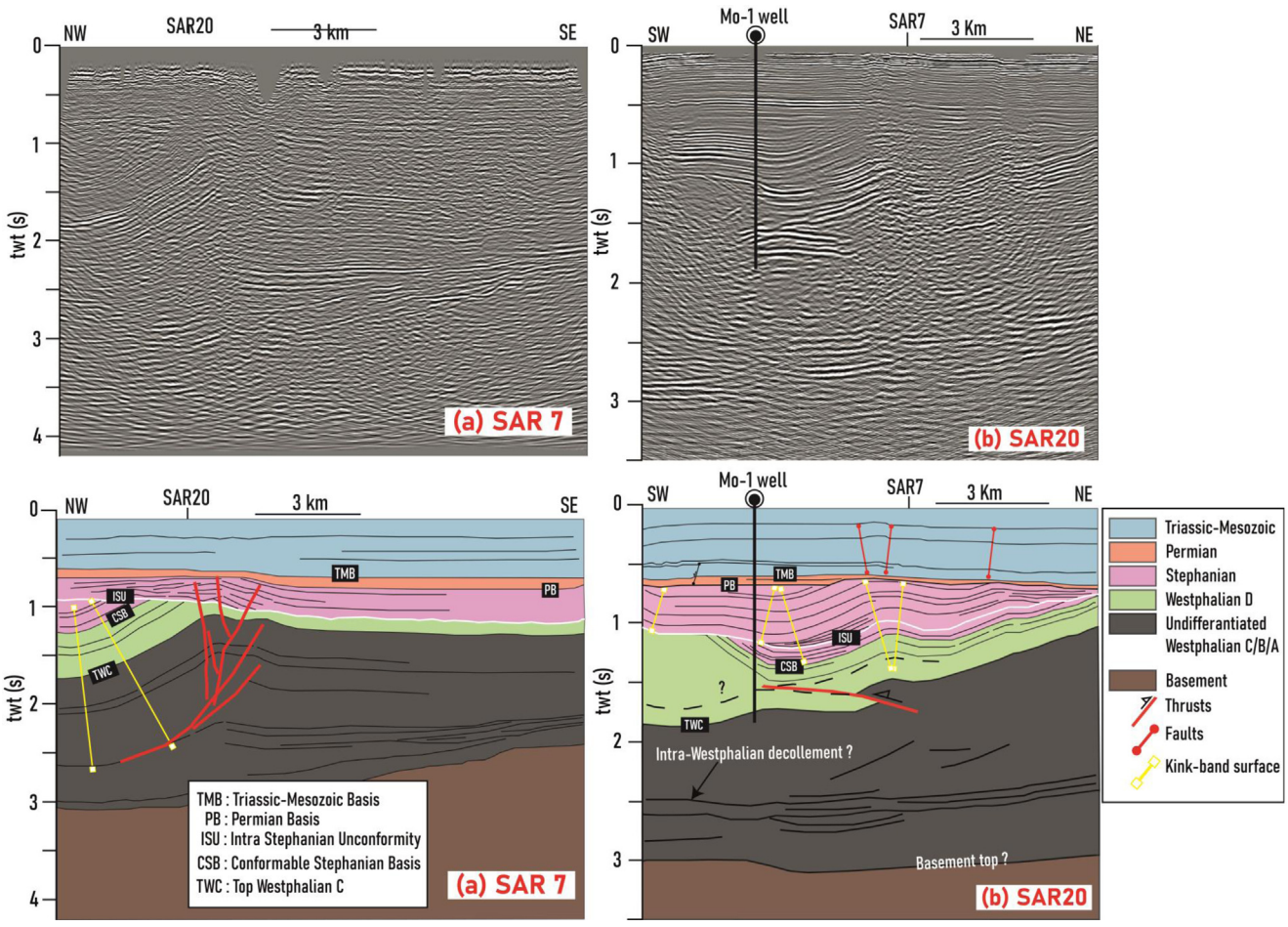

Fig. 10. (a) Uninterpreted and interpreted migrated SAR07. (b) Uninterpreted and interpreted migrated SAR20. The SAR7 highlights the Alsting fold as a pop-up anticline, probably a positive flower structure. The SAR20 shows that the Stephanian sub-sequence overlying the ISU is made up of typical growth strata.

present almost everywhere in the Permian sequence of the Nahe syncline. As the algorithm assumes that the long wavelength anomalies correspond to the basement anomalies, the algorithm could have confused their anomalies with the signature of the basement. The other interesting basement high is located at the PaMTF. This might correspond to the basement involved in the PaMTF as shown by Hemelsdaël *et al.* (2023).

Regarding the basement deeps, The Landstühl well (Land-1) located in the circular shape deep crosses the Permian basis at 3 km (Becker and Schäfer, 2020; 2021), and the seismic line A (Schäfer, 2011) predict 3 km of Westphalian-Stephanian under this Permian basis. These two observations predict a 6 km depocenter, matching well with the map. Becker and Schäfer (2020) suggest the Permian sequence is made up of half-graben bounded by NW-SE transfer faults. The geometry and the orientation of the deeps (Fig. 6) may indicate that they are bounded by NW-SE faults. In this case, such faults might affect the basement top as well. The other basement deep which seems to be controlled by the NW-SE fault is located above the Saarbrücken city. In the north-eastern part of the LCB, the elongated NE-SW basement deep in the north-eastern part of the LCB aligned with the Landroff syncline. Within this deep, the seismic line RE01 highlights a Stephanian depocenter with the basis located at almost 4 km, overlaying a thick Westphalian sequence whose basis is probably deeper than 6 km. The depth and the structure observed on this seismic line agrees with the map.

In the southwestern part of the LCB, the case of the Gironville-Francheville deep, located between the CoF and the MoF, correspond to a thick (3s-twt thick) Westphalian syncline overlain by the Stephanian sequence controlled by the ToF (Fig. 6, Hemelsdaël *et al.*, 2023). Furthermore, this Figure 6 shows the basement top at 3.3 s(twt) fitting with the depth predicted by the map. According to the interpretation on Figure 7 from Hemelsdaël *et al.* (2023), the Meligny and Chevraumont deeps correspond to the Gironville-Franchville depocenter. Our map show that both deeps seem to be laterally offset, probably indicating a sinistral displacement on the CoF. Meligny well (Mny) does not reach the Westphalian but shows a thick Triassic-Mesozoic until 1.75 km. The Chv well cross the Stephanian until 2.5 km. Hemelsdaël *et al.* (2023) interpreted the basement top at 2.5 s(twt) suggesting a less important global thickness than the 5 km predicted by our map. Yet, our map and the seismic lines in Hemelsdaël *et al.* (2023) both highlight the basement structuration. This structuration

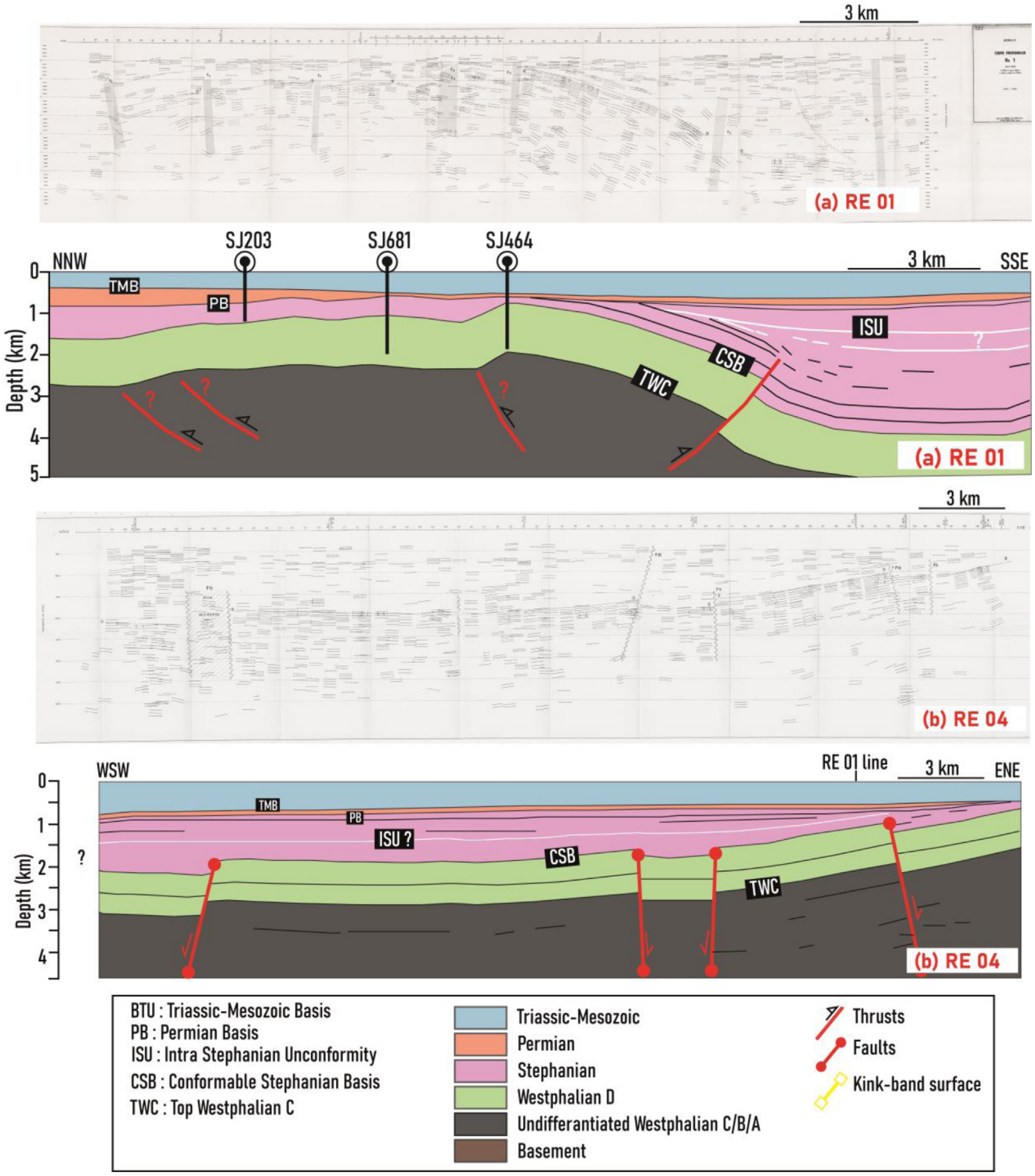

Fig. 11. (a) Uninterpreted and interpreted migrated RE01. (b) Uninterpreted and interpreted migrated RE04. The RE01 highlights the Merlebach anticline as a SE-vergent thrust fold with a possible back thrust in the piggyback syncline. Note the important thickening of the Stephanian sequence in the Landroff syncline. The RE04 highlights NW-SE syn- Stephanian sedimentary faults.

can be related to the folding of the basement when the basin underwent compression or simply represents the inherited basement structuration. The L.Ge-1 well, located on the border of this depocenter, encounters 1.4 km of Stephanian-permian sequence and 1.3 km of Permian. Our map predicts a thicker sedimentary cover (around 6 km), which can suggest that there is a 3 km thickness of the Stephanian-Westphalian formations before reaching the basement top. Furthermore, by making the seismic-to-well tie on the Toul 12 with this well (Fig. 4b), it appears that the Permian basis is likely located at 2 s, and the

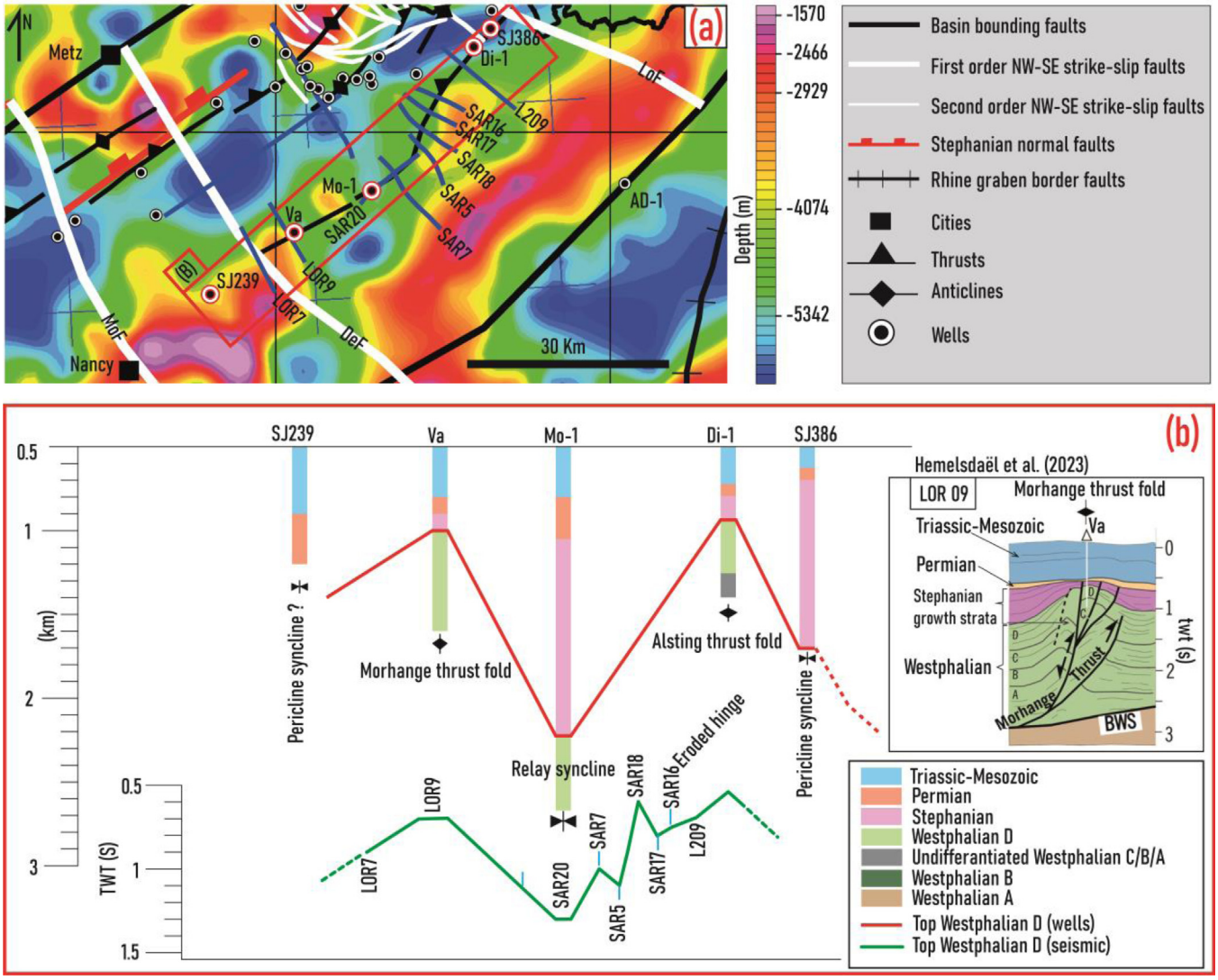

Fig. 12. (a). Location of the different seismic lines and wells highlighted in b. (b). Two-Way-Time (from seismic) and depth profile of the Top Westphalian D from the Alsting to the Morhange thrust-folds highlighting the Morhange growth syncline between the two thrust-folds and the same growth strata on the LOR9 seismic line from Hemelsdaël *et al.* (2023).

Stephanian basis at 3.2 s, which is also in agreement with the thickness ranges predicted by the map.

5.2.2 The fold hinge area, the piggyback and the growth syncline

The different tectono-sedimentary evolution recorded at the fold hinge and in the synclines allow to explain some of the thickness variations trends observed for the Stephanian-Permian formations. The low thickness observed at the fold hinge areas is explained by the post-compressional erosion of the folded sub-sequence under the ISU and to the low thickness or the non-deposition of the upper sub-sequence of drape strata overlaying the ISU. On the contrary, the high thickness of the Early Stephanian observed in the piggyback syncline is due to the preservation of both sub-sequences. Pruvost (1934) map highlights that the erosion at the Westphalian-Stephanian limit is more important around the Saarbrucken thrust fold as the Holz-conglomerate rests on the C and B. On the SAR 5 (Fig. 9b), the ISU rests on the Westphalian D and C while it rests only on the Westphalian D in the other seismic lines, proving different local erosion rates under the Holz-conglomerate as highlighted by Pruvost (1934).

The low Permian thickness observed at the hinge area is due to post-depositional erosion. The low Permian thickness observed at the hinge area is due to the Permian and Triassic erosion. Furthermore, the geometry characteristic of the Mo-1 syncline revealed by the SAR20 (Fig. 11b) and the lateral evolution of the depth of the Stephanian basis reflection from the Alsting to the Morhange thrust folds (Fig. 12) allows to conclude that the Morhange syncline is a relay growth syncline. The fan-shape geometry of the Early Stephanian reflections explains the high thickness (1.2 km) observed on the Mo-1 well. At the Morhange hinge (Fig. 12), the low thickness observed on Va well is explained by the thinning of the Stephanian (from 0.5 s in the Landroff syncline to 0.2 s at the Morhange hinge) as interpreted by Hemelsdaël *et al.* (2023). The same fan-geometry is observed for the thick (2 km) Stephanian sequence on the RE 01 (Fig. 11b).

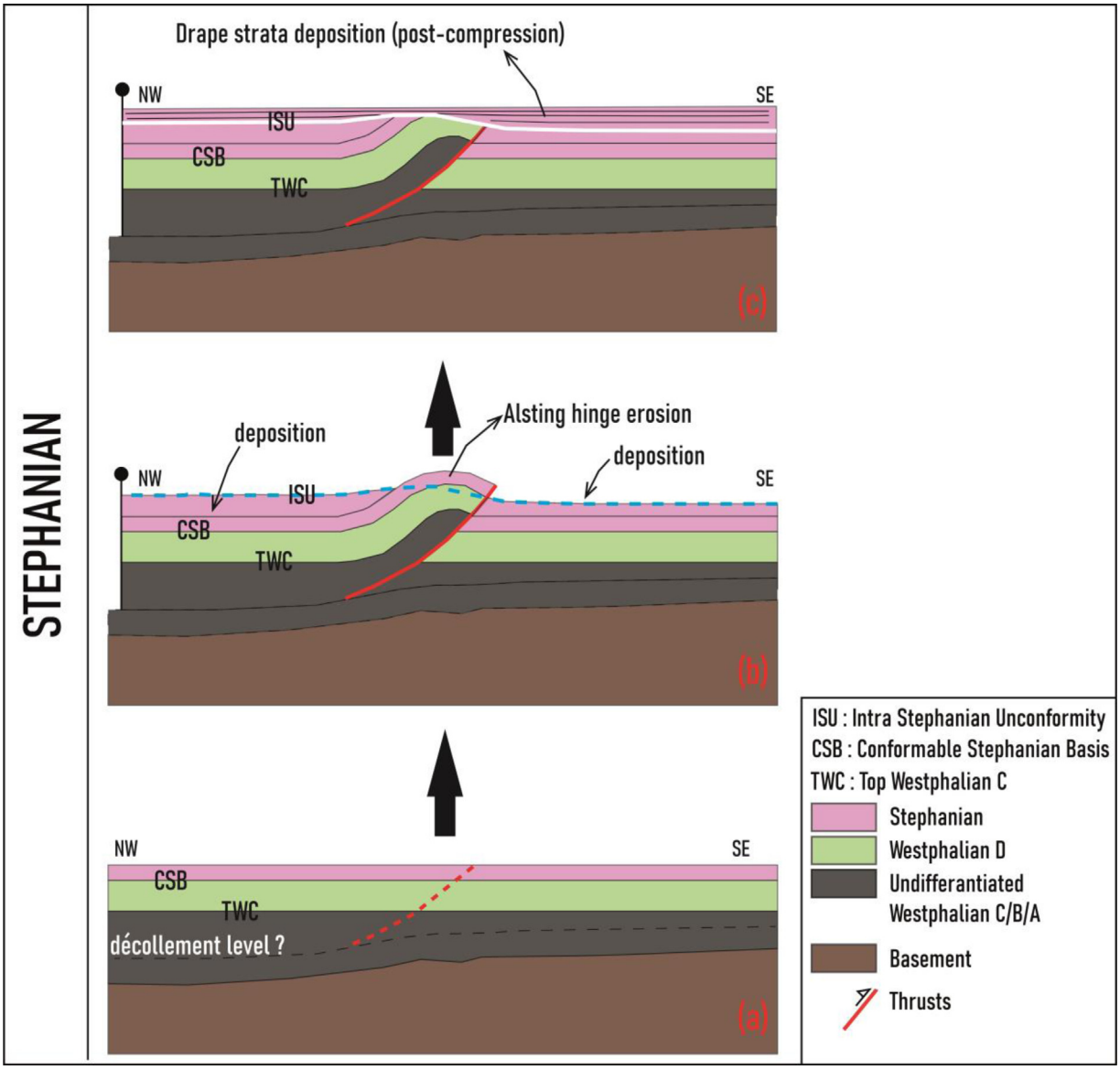

Fig. 13. Proposal of a tectono-sedimentary evolution of the Alsting anticline. The cross-sections are not in scale. (a) Continuous deposition from the Westphalian until the Early Stephanian lower sub-sequence. (b) Thrusting and folding of the Westphalian-Stephanian sub-sequence leading to the formation of the Alsting thrust fold and its subsequent uplift and erosion. (c) Renew of subsidence and deposition of the Upper Stephanian sub-sequence as drape strata.

Therefore, another explanation of the high thickness of the Stephanian sequence in the syncline area and their low thickness at the hinge area might be due to the growth nature of these strata.

For the Triassic-Mesozoic sequence, the thickness variations are linked to the post-variscan history. The less important thickness of these formations in the north-east of the LCB are due to a more important erosion of the Paris basin formations (Blaise *et al.*, 2014; Izart *et al.*, 2016) by using the 1D burial and thermal modelling of the boreholes EST433 (close to Germisay) and the Rn8 (close to Nancy).

5.2.3 The NW-SE faults

The role of NW-SE faults on the Permian and Stephanian sequences thickness variations have been largely been described in the LCB and SNCB (Pruvost, 1934; Engel, 1985; Stollhofen, 1998, Donsimoni, 1981, Becker and Schäfer, 2020, 2021; Hemelsdaël *et al.*, 2023). The only seismic lines in our dataset that can image such faults are the SAR20 and the RE04 as they are oriented perpendicular to the fault's orientation. For the Permian sequence, the two lines show that the strata drape the folded and eroded anticline, they are not controlled by any NW-SE faults. Furthermore, some of these NW-SE syn-sedimentary normal faults are visible on the RE04 line (Fig. 11b) in the Lower Stephanian under the ISU.

However, it is difficult to assess the syn-sedimentary activity of the LoF and the DeF only with well data. The SJ239 located between these two faults (Fig. 4a), show a 300 m thick for the Permian formations (Fig. 7). This high thickness might indicates the effect of one of these faults. Yet, the well is in a syncline which can explain a high preservation of the Permian formations. Likewise, even if the SJ244 shows a thicker (120 m) Permian

than in the SJ234 (10 m) (Fig. 7), it is difficult to relate this high thickness to the fault activity since the SJ244 is in a relay syncline (Fig. 4a). Moreover, the SJ234 is located at the PaMTF hinge, which underwent an important erosion which can explain the low Permian thickness (10 m). This erosion may explain the absence of the Stephanian formations in this well. Therefore, the presence of such faults and their role in thickness variation is much localised in the LCB.

5.3 Tectono-sedimentary evolution of the Alsting thrust-fold

Considering that there is no thickening of the Westphalian strata along the thrust, any visible preserved normal throw, and considering the geometry of the thrust, the Alsting thrust-fold is interpreted as a fault-propagation fold. The fact that its thrust soles out within the Westphalian sequence (at 2.2 s twt, according to our interpretation) may indicate a thin skin-deformation style in this area. The SAR 7 (Fig. 10a) on which the Westphalian-basement interface is better imaged (at 3 s) shows no deformation of the basement, supporting our suggestion of a thin-skin deformation style.

Furthermore, as regard to the timing of the Alsting fold, the drape sequence that deposited after the ISU development leads to conclude that the fold was formed during the Early Stephanian. Therefore, a tectono-sedimentary evolution of the Alsting thrust fold is proposed on Figure 13. After a continuous sedimentation from the Westphalian until the Early Stephanian, the LCB was affected by the Variscan compression leading to the formation of the Alsting thrust fold (Fig. 13a). The Alsting hinge was uplifted to the surface and underwent an important erosion leading to the ISU formation (Fig. 13b). The sediment eroded probably nourished the back limb and fore limb synclines. Later, sedimentation resumed, and the fold was draped by the Stephanian upper sub-sequence (Fig. 13c). The fan-shape geometry of these strata on SAR20 (Fig. 10b) suggest that sedimentation took place during the fold growth (Suppe and Medwedeff, 1990; Suppe *et al.*, 1992; Hardy and Poblet, 1994; Ford *et al.*, 1997; Butler *et al.*, 2019).

Yet, this scenario must be investigated further since the fan-shape geometry is not observed on all the crosslines which rather suggest a post-compression deposition (drape strata). Nevertheless, our intra-Stephanian compression inferred fit with the proposal of Engel (1985) and Hertle and Littke (2000) which suggests that the Saarbrücken and the Simon thrust-fold formed during a Stephanian compression. This compression event corresponds to the Franconian compressional phase during the Stephanian or at the Stephanian-Autunian boundary (Stille, 1920; Pruvost, 1934; Kneuper, 1964; Gebhardt *et al.*, 1991). Thus, the Stephanian period was not governed by a global extension as proposed by many authors before. The formation of the Stephanian half graben in the south-western part of the LCB (Hemelsdaël *et al.*, 2023) might have happened during the deposition of the drape strata overlying the ISU.

6 Conclusions

The study of gravity data has allowed to map the MHF and the top basement geometry while the 2D seismic lines and wells has allowed to constrain the tectono-sedimentary evolution of the Alsting thrust fold. These observations have led to the following conclusions:

- The MHFZ is a complex fault zone throughout the LCB and the SNCB with several secondary branching faults which orientations varies laterally.
- The basement top map has shown the presence of basement highs (−1.5 km) and deeps (−6.5 km) trending NE-SW, NNE-SSW to N-S and NW-SE. The NE-SW deeps align with the piggyback and frontal synclines while the some of the NW-SE deeps align with the known NW-SE Permian half-graben.
- The Alsting thrust-fold is a fault-propagation fold which formed during Stephanian. Following its exhumation, the fold underwent an erosion leading to the development of an intra-Stephanian unconformity (ISU) before the last phase of Stephanian subsidence.
- During this subsidence phase, the fold was sealed by drape strata (post-compressional) overlaying the ISU. However, on SAR 20 seismic line striking parallel to the Alsting thrust fold, the Stephanian growth strata overlaying the ISU may suggest that the Alsting uplift was still active. This statement must be studied further.
- The combination of gravity, seismic and well data analysis has allowed to decipher a different geological history of the LCB during Stephanian and have helped to constrain the basement top structure which has received less attention until now.

Acknowledgments

This work is part of the REGALOR (REssources GAzières de LORraine) project, which was cofounded by the FEDER (Fond Européen de DEveloppement Régional) and the Région Grand-Est. The project was conducted by the Georessources laboratory and la Française de l'Energie (FDE) company. FDE is warmly thanked for providing the seismic data analysed in this work. We would like to thank Stéphane BRUSSET and an anonymous reviewer for their corrections and suggestions that greatly improved the manuscript.

References

Allemand P, Lardeaux JM, Dromart G, Ader M. 1997. Late orogenic extension and development of intracontinental basins: the Cévennes stephanian basin. Geodin Acta 10: 70–80. https://doi.org/10.1080/09853111.1997.11105294.

Alpern B, Choffe M, Lachkar G, Liabeuf JJ. 1969. Synthèse des zonations palynologiques des bassins houillers de Lorraine et de Sarre. Rev Micropaleontol 4: 217–221.

Anderle, HJ. 1986. The evolution of the South Hunsrück and Taunus Borderzone. Tectonophysics 137: 101–114. https://doi.org/10.1016/0040(87)90317-9.

Aretz M, Herbig HG, Wang XD, Gradstein FM, Agterberg FP, Ogg JG. 2020. The Carboniferous Period. In Geologic Time Scale 2020, pp.: 811–874: Elsevier. https://doi.org/10.1016/B978-0-12-824360-2.00023-1.

Arthaud F, Matte P. 1977. Late-Palaeozoic strike-slip faulting in southern Europe and northern Africa: Result of a right-lateral shear-zone between the Appalachians and the Urals. Geol Soc Am

Bull 88: 1305–1320. https://doi.org/10.1130/0016-7606(1977)88<1305:LPSFIS>2.0.CO;2.

Averbuch O, Piromallo C. 2012. Is there a remnant Variscan subducted slab in the mantle beneath the Paris basin? Implications for the late Variscan lithospheric delamination process and the Paris basin formation. Tectonophysics 558–559: 70–83. https://doi.org/10.1016/j.tecto.2012.06.032.

Beccaletto L, Averbuch O, Izart A. 2019. The Lorraine-Saar basin (E France) in the framework of the Variscan Orogeny: structure and tectono-sedimentary evolution. Abstracts, 19th International Congress on the Carboniferous and Permian, Cologne.

Becker A, Schäfer A. 2020. Depth contour maps for the Rotliegend Formations of the central Saar-Nahe Basin, SW Germany. – Z dt G. Geowiss 171, 4: 429–442. https://doi.org/10.1127/zdgg/2020/0253.

Becker A, Schäfer A. 2021. Entwicklung des Saar-Nahe-Beckens im späten Paläozoikum. Jahresberichte und Mitteilungen des Oberrheinischen. Geologischen Vereins 103: 211–233. https://doi.org/10.1127/jmogv/103/0006.

Bertrand P. 1928. L'échelle stratigraphique du terrain Houiller de la Sarre et de la Lorraine. *CR*. Congr. Stratigr. Carbonifère. Heerlen, pp. 83–116.

Blaise T, Barbarand J, Kars M, *et al.* 2014. Reconstruction of low burial (b100 C) in sedimentary basins : a comparison of geothermometers sensibility in the intracontinental Paris Basin. Mar Pet Geol 53: 71–87. https://doi.org/10.1016/j.marpetgeo.2013.08.019.

Blès JL, Lozes J. 1980. Gazéification in situ du charbon, site de Faulquemont, étude structurale. BRGM Report 80SGN427GEO, Annexes 20, pp. 28.

Brun JP, Gutscher MA, dekorp-ecors teams. 1992. Deep crustal structure of the Rhine Graben from dekorp-ecors seismic reflection data: A summary. Tectonophysics 208: 139–147. https://doi.org/10.1016/0040(92)90340-C.

Burg JP, Van Den Driessche J, Brun JP. 1994. L'extension syn- à post-épaississement de la chaîne Varisque en Europe occidentale: modalités et conséquences. Géologie de la France 3: 33–51.

Burger K, Hess JC, Lippolt HJ. 1997. Tephrochronologie mit Kaolin-Kohlentonsteinen: Mittel zur Korrelation paralischer und limnischer Ablagerungen des Oberkarbons. Hannover; Stuttgart. Bundesanstalt für Geowissenschaften und Rohstoffe [etc.];. In: Kommission E. ed. Schweizerbart'sche Verlagsbuchhandlung. (Vol 147,pp.39, 2 zganj. f. pril.).

Butler RWH, Maniscalco R, Pinter PR. 2019. Syn-kinematic sedimentary systems as constraints on the structural response of thrust belts: re-examining the structural style of the Maghrebian thrust belt of Eastern Sicily. Int J Geosciences 138: 371–389. https://doi.org/10.3301/IJG.2019.11.

Corsini M, Rolland Y. 2009. Late evolution of the southern European Variscan belt: Exhumation of the lower crust in a context of oblique convergence. *CR* Géoscience 341: 214–223. https://doi.org/10.1016/j.crte.2008.12.002.

Djarar L, Wang H, Guiraud M, *et al.* 1996. The Cévennes Stephanian basin (Massif Central): an example of relationships between sedimentation and late-orogenic extensive tectonics of the Variscan belt. Geodin Acta 9, 5: 193–221. https://doi.org/10.1080/09853111.1996.11105286.

Donsimoni M. 1981. Le bassin houiller lorrain, Synthèse géologique. Mémoire. BRGM 117, pp. 99.

Drozdzewski G, Juch D. 1992. Der Saarbrücker Sattel – eine Blumenstruktur? – Nachr Dt Geol Ges 48: 90–91.

Edel JB, Schulmann K. 2009. Geophysical constraints and model of the "Saxothuringian and Rhenohercynian subductions – magmatic arc system" in NE France and SW Germany. Bull Soc Géol Fr 180: 545–558. https://doi.org/10.2113/gssgfbull.180.6.545.

Engel H. 1985. Zur Tektogenese des Saarbrücker Hauptsattels und der Südlichen Randüberschiebung. In: Drozdzewski G, Engel H, Wolf R, Wrede V. Eds eds., Beiträge zur Tiefentektonik westdeutscher Steinkohlenlagerstätten, Krefeld, pp. 217–235.

Essa KS, Munschy M, Youssef, MAS, Ess El Din A. 2022. Aeromagnetic and Radiometric Data Interpretation to Delineate the Structural Elements and Probable Precambrian Mineralization Zones: a Case Study, Egypt. Mining, Metallurgy & Exploration Explor 39: 2461–2475. https://doi.org/10.1007/s42461-022-00675-0.

Essa KS, Nady AG, Mostafa MS, Elhussein M. 2018. Implementation of potential field data to depict the structural lineaments of the Sinai Peninsula, Egypt. J Afr Earth Sci 147: 43–53. https://doi.org/10.1016/j.jafrearsci.2018.06.013.

Faure M, Mézème EB, Duguet M, Cartier C, Talbot JY. 2005. Paleozoic tectonic evolution of medio-Europa from the example of the French Massif Central and Massif Armoricain. Journal of the Virtual Explorer, 19(5),): 1–25. https://dx.doi.org/10.3809/jvirtex.2005.00120.

Faure M. 1995. Late orogenic carboniferous extensions in the Variscan French Massif Central. Tectonics, American Geophysical Union (AGU), 14 (1),): pp.132–153. https://doi.org/10.1029/94TC02021.

Ford M, William EA, Hardy S. 1997. Progressive evolution of a fault-related fold pair from growth strata geometries, Sant Llorenç de Maruys, SE Pyrenees. J Struc Geol 19: 413–441. https://doi.org/10.1016/S0191(96)00116-2.

Franke W. 2000. The mid-European segment of the Variscides: tectonostratigraphic units, terrane boundaries and plate tectonic evolution. In: Franke W, Haak V, Oncken O, and Tanner D, (Eds.). Orogenic Processes: Quantification and Modelling in the Variscan Belt. Special Publication 179. London: Geol Soc, pp. 35–62. https://doi.org/10.1144/GSL.SP.2000.179.01.05.

Franke W. 2014. Topography of the Variscan orogen in Europe: failed-not collapsed. Int *J* Earth Sci 103: 1471–1499. https://doi.org/10.1007/s00531-014-1014-9.

Ganguli SS, Pal SK, Singh SL, Rama Rao JV, Balakrishna B. 2020. Insights into crustal architecture and tectonics across Palghat Cauvery Shear Zone, India from combined analysis of gravity and magnetic data. Geol J 55: 1–19. https://doi.org/10.1002/gj.4041.

Gébelin A, Roger F, Brunel M. 2009. Syntectonic crustal melting and high-grade metamorphism in a transpressional regime, Variscan Massif Central, France. Tectonophysics 477: 229–243. https://doi.org/10.1016/j.tecto.2009.03.022.

Gebhardt U, Schneider J, Hoffmann N. 1991. Modelle zur Stratigraphy und Beckenentwicklung im Rotliegenden der Norddeutschen Senke. Geol. Jb. A 127: 405–427, Hannover.

Geologische Ubersichkarte von Saar (Geological map from Saar). 1979. Scale 1/200000 Saarbrücken-Hannover CC 7102, Bundesrepublik Deutschland.

Guillocheau F, Robin C, Allemand P, *et al.* 2000. Meso-Cenozoic geodynamic evolution of the Paris Basin: 3D stratigraphic constraints. Geodin Acta 13: 189–245. https://doi.org/10.1080/09853111.2000.11105372.

Hardy S, Poblet J. 1994. Geometric and numerical model of progressive limb rotation in detachment folds. Geology 22: 371–

374. https://doi.org/10.1130/0091-7613(1994)022%3C0371:GANMOP%3E2.3.CO;2.

Hemelsdaël R, Averbuch O, Beccaletto L, *et al.* 2023. A deformed wedge-top basin inverted during the collapse of the Variscan belt: The Permo-Carboniferous Lorraine Basin (NE France). Tectonics 42, : e2022TC007668. https://doi.org/10.1029/2022TC007668.

Henk A. 1993. Late orogenic Basin evolution in the Variscan internides: the Saar-Nahe Basin, southwest Germany. Tectonophysics 223: 273–290. https://doi.org/10.1016/0040-1951(93)90141-6.

Hertle M, Littke R. 2000. Coalification pattern and thermal modelling of the Permo-Carboniferous Saar Basin (SW-Germany). Int *J* Coal Geol 42: 273–296. https://doi.org/10.1016/S0166(99)00043-9.

Izart A, Barbarand J, Michels R, Privalov VA. 2016. Modelling of the thermal history of the Carboniferous Lorraine Coal Basin: Consequences for coal bed methane. Int J Coal Geol 168: 253–274. https://doi.org/10.1016/j.coal.2016.11.008.

Izart A, Opluštil S, Michels R, Voigt S, Barbarand J, Blaise T, Laurin J, Schmitz M, Hartkopf C, Allouti S, Hemelsdael R *et al.* 2025. New high precision U-Pb zircon ages of the Saar-Lorraine (SW Germany-NE France) Basin. – Int J Coal Geol. https://doi.org/10.1016/j.coal.2025.104724.

Izart A, Palain C, Malartre F, Fleck S, Michels R. 2005. Paleoenvironments, paleoclimates and sequences of Westphalian deposits of Lorraine coal basin (Upper Carboniferous, NE France). Bull Soc Géol Fr 176: 301–315. https://doi.org/10.2113/176.3.301.

Juch D, Roos WF, Wolff M. 1994. Kohleninhaltserfassung in den westdeutschen Steinkohlenlagerstätten. – Fortschritte in der Geologie von Rheinland und Westfalen. Krefeld 38, : 189–307.

Kelch HJ, Reible P. 1976. Bescheibung der Spülproben and Kerne der Bohrung Saar 1. Geol J A27: 29–89.

Kneuper G. 1964. Grundzüge der Sedimentation und Tektonik im Oberkarbon des Saarbrücker Hauptsattels. Oberrheinische geologische Abhandlungen 13: 1–49.

Königer S, Lorenz V, Stollhofen H. 2002. Origin, age and stratigraphic significance of distal fallout ash tuffs from the Carboniferous-Permian continental Saar-Nahe Basin (SW Germany). Int J Earth Sci 91: 341–356. https://doi.org/10.1007/s005310100221.

Königer S, Lorenz V. 2002. Geochemistry, tectonomagmatic origin and chemical correlation of altered Carboniferous-Permian fallout ash tuffs in southwestern Germany. Geological Magazine, 139 (05). https://doi.org/10.1017/S0016756802006775.

Korsch RJ, Schäfer A. 1995. The Permo-Carboniferous Saar-Nahe Basin, south-west Germany and north-east France: basin formation and deformation in a strike-slip regime. Geol Rundsch 84: 293–318. https://doi.org/10.1007/BF00260442.

Kroner U, Mansy JL, Mazur S, *et al.* 2008. Variscan tectonics. In: McCann T., (Eed.), The geology of Central Europe. Geological Society, London: Geological Society, pp. 599–664.

Kroner U, Romer RL. 2013. Two plates – Many subduction zones: The Variscan orogeny reconsidered. Gondwana Res 24: 298–329. https://doi.org/10.1016/j.gr.2013.03.001.

Lardeaux JM, Schulmann K, Faure M, *et al.* 2014. The Moldanubian Zone in the French Massif Central, Vosges/Schwarzwald and Bohemian Massif revisited: differences and similarities. Geological Society, London, Special Publications 405: 7–44. https://doi.org/10.1144/SP405.14.

Laveine JP. 1974. Précisions sur la répartition stratigraphique des principales espèces végétales du Carbonifère supérieur de Lorraine. C.R. Acad. Sci. Fr. 278: 851–854.

Le Solleuz A, Doin MP, Robin C, Guillocheau F. 2004. From a mountain belt collapse to a sedimentary basin development. 2-D thermal model based on inversion of stratigraphic data in the Paris Basin. Tectonophysics 386: 1–27. https://doi.org/10.1016/j.tecto.2004.03.006.

Lippolt HJ, Hess JC, Raczek I. 1989. Isotopic evidence for the stratigraphic position of the Saar-Nahe Rotliegende volcanism, II. Rb-Sr investigations. – N. Jb. Geol. Paläont. Mh., 1989: 539–552.

Mazur S, Aleksandrowski P, Gągała Ł,, *et al.* 2020. Late Palaeozoic strike-slip tectonics versus oroclinal bending at the SW outskirts of Baltica: case of the Variscan belt's eastern end in Poland. Inter J Earth Sc 109: 1133–1160. https://doi.org/10.1007/s00531-019-01814-7.

McCann T, Pascal C, Timmerman MJ, *et al.* 2006. Post-Variscan (end Carboniferous-Early Permian) basin evolution in Western and Central Europe. Geological Society, London, Memoirs 32: 355–388. https://doi.org/10.1144/GSL.MEM.2006.032.01.22.

Menning M, Bachtadse V. 2012. Magnetostratigraphie und globale Korrelation des Rotliegend innervariscischer Becken. In: Stratigraphie von Deutschland X. Rotliegend. Teil I: Innervariscische Becken. Schriftenreihe der Deutschen Gesellschaft für Geowissenschaften, v. 61, p.: 176–203. https://gfzpublic.gfzpotsdam.de/pubman/item/item_247906.

Merry LL. 1967. Découverte de nouveaux tonsteins dans le Westphalien de Lorraine. C R Acad Sc Fr 264: 2440–2442.

Oncken O, von Winterfeld C, Dittmar U. 1999. Accretion of a rifted passive margin: The Late Paleozoic Rhenohercynian fold and thrust belt (Middle European Variscides). Tectonics 18: 75–91. https://doi.org/10.1029/98TC02763.

Oncken O. 1998. Evidence for precollisional subduction erosion in ancient collisional belts: The case of the Mid-European Variscides. Geology 26, 12: 1075–1078. https://doi.org/10.1130/0091(1998)026%3C1075:EFPSEI%3E2.3.CO;2.

Prijac C, Doin MP, Gaulier JM, Guillocheau F. 2000. Subsidence of the Paris Basin and its bearing on the late Variscan lithosphere evolution: a comparison between Plate and Chablis models. Tectonophysics 323: 1–38. https://doi.org/10.1016/S0040-1951(00)00100-1.

Pruvost P. 1934. Bassin houiller de la Sarre et de la Lorraine, t. III: Description géologique. Etudes gîtes minéraux, France, Lille, Imprimerie Danel.

Privalov V, Pironon J, Izart A, Michels R, Panova O. 2015.A new tectonic model for the late paleozoic evolution of the lorraine-saar coal-bearing basin (France/Germany). Tekton. Stratigr. 0: 40–50.

Schäfer A. 1989. Variscan molasse in the Saar-Nahe Basin (W-Germany), Upper Carboniferous and Lower Permian. Geol Rundsch 78: 499–524. https://doi.org/10.1007/BF01776188.

Schäfer A. 2011. Tectonics and sedimentation in the continental strike-slip Saar-Nahe Basin (Carboniferous-Permian, West Germany). Zeitschrift der Deutschen Gesellschaft für Geowissenschaften 162: 127–155. https://doi.org/10.1127/1860-1804/2011/0162-0127.

Skrzypek E, Schulmann K, Tabaud AS, Edel JB. 2014. Palaeozoic evolution of the Variscan Vosges Mountains. Geological Society of London, Special Publication 405: 45–75. https://doi.org/10.1144/SP405.8.

Smith RS, Thurston, JB, Dai Ting-fan, and MacLeod LN. 1998. The improved source parameter imaging method. Geophysical Prospecting 46: 141–151. https://doi.org/10.1046/j.1365-2478.1998.00084.x.

Spector A, Grant FS. 1970. Statistical models for interpreting aeromagnetic data. Geophysics 35: 293–302. https://doi.org/10.1190/1.1440092.

Stephan T, Kroner U, Hahn T, Hallas P, Heuse T. 2016. Fold/cleavage relationships as indicator for late Variscan sinistral transpression at the Rheno-Hercynian-Saxo-Thuringian boundary zone, Central European Variscides. Tectonophysics 681: 250–262. https://doi.org/10.1016/j.tecto.2016.03.005.

Stille H. 1920. Uber Alter und Art der Phasen Variscischer Gebirgsbildung. Nachr. Gött. Gesel. Math-Phys KL 1920: 218–224.

Stollhofen H. 1998. Facies architecture variations and seismogenic structures in the Carboniferous-Permian Saar-Nahe Basin (SW Germany): evidence for extension-related transfer fault activity. Sedimentary Geology 119: 47–83. https://doi.org/10.1016/S0037(98)00040-2.

Suppe J, Chou GT, Hook SC. 1992. Rates of folding and faulting determined from growth strata. In: McClay KR., (Eed.), Thrust tectonics. Springer Netherlands, Dordrecht: Springer Netherlands, pp. 105–121. https://doi.org/10.1007/978-94-011-3066-0_9.

Suppe, J., Medwedeff, D. A., 1990. Geometry and kinematics of fault-propagation folding. Eclogae Geol. Helv 83, : 409–454.

Tabaud AS, Whitechurch H, Rossi P, Schulmann K, Guerrot C, Cocherie A. 2014. Devonian-Permian magmatic pulses in the northern Vosges Mountains (NE France): result of continuous subduction of the Rhenohercynian Ocean and Avalonian passive margin. Geological Society, London, Special Publications 405: 197–223. https://doi.org/10.1144/SP405.12.

Teichmüller MR. 1966. Die Inkohlung im saar-lothringer Karbon, verglichen mit der im Ruhrkarbon. Zeitschrift der deutschen geologischen Gesellschaft, 117: 243–279, Hannover.

Termier P. 1923. Contribution à la connaissance des tonsteins du Houiller de la Sarre. Bull Soc Géo. Fr 4, : 23–45.

Thurston JB, Smith RS. 1997. Automatic conversion of magnetic data to depth, dip, and susceptibility contrast using the SPI(TM) method. Geophysics 62: 807–813. https://doi.org/10.1190/1.1444190.

Villemin T. 1987. Comparaison des densités de facturation à différentes échelles : exemple du bassin houiller lorrain. Geodin Acta 1: 147–157. https://doi.org/10.1080/09853111.1987.11105133.

Voigt S, Schindler T, Tichomirowa M, Käßner A, Schneider JW, Linnemann U. 2022. First high-precision U-Pb age from the Pennsylvanian-Permian of the continental Saar-Nahe Basin, SW Germany. International Journal of Earth Sciences, 111(7),): 2129–2147. https://doi.org/10.1007/s00531-022-02222-0.

Zahorec P, Papčo J, Pašteka R, *et al.* 2021. The first pan-Alpine surface-gravity database, a modern compilation that crosses frontiers. Earth Syst Sci Data 13: 2165–2209. https://doi.org/10.5194/essd-13-2165-2021.

Zimmerle W. 1976. Petrographische Beschreibung und Deutung der erbohrten Schichten. In: Birenheide R,, *et al.* (1976. Die Tiefbohrung Saar 1: Geol. Jb., A 27: 91–305, Hannover (B. Anst. Bodenforsch.).

Cite this article as: Mombo Mouketo M, Géraud Y, Diraison M, Allouti S, Izart A, Essa K, Bossennec C, Nassif F. 2026. Structural organization of the Lorraine coal basin and formation of the Alsting thrust fold, *BSGF - Earth Sciences Bulletin* 197: 5. https://doi.org/10.1051/bsgf/2025028